Sentryn Acts with a Subset of Active Zone Proteins To Optimize the Localization of Synaptic Vesicles in *Caenorhabditis elegans*

Stacey L. Edwards,*[,1] Logan M. Morrison,*[,1] Laura Manning,[†] Natalia Stec,* Janet E. Richmond,[†] and Kenneth G. Miller*[,2]

*Genetic Models of Disease Laboratory, Oklahoma Medical Research Foundation, Oklahoma 73104; and [†]Department of Biological Sciences, University of Illinois at Chicago, Illinois 60607

ABSTRACT Synaptic vesicles (SVs) transmit signals by releasing neurotransmitters from specialized synaptic regions of neurons. In the synaptic region, SVs are tightly clustered around small structures called active zones. The motor KIF1A transports SVs outward through axons until they are captured in the synaptic region. This transport must be guided in the forward direction because it is opposed by the dynein motor, which causes SVs to reverse direction multiple times en route. The core synapse stability (CSS) system contributes to both guided transport and capture of SVs. We identified Sentryn as a CSS protein that contributes to the synaptic localization of SVs in *Caenorhabditis elegans*. Like the CSS proteins SAD Kinase and SYD-2 (Liprin-α), Sentryn also prevents dynein-dependent accumulation of lysosomes in dendrites in strains lacking JIP3. Genetic analysis showed that Sentryn and SAD Kinase each have at least one non-overlapping function for the stable accumulation of SVs at synapses that, when combined with their shared functions, enables most of the functions of SYD-2 (Liprin-α) for capturing SVs. Also like other CSS proteins, Sentryn appears enriched at active zones and contributes to active zone structure, suggesting that it is a novel, conserved active zone protein. Sentryn is recruited to active zones by a process dependent on the active zone-enriched CSS protein SYD-2 (Liprin-α). Our results define a specialized group of active zone enriched proteins that can affect motorized transport throughout the neuron and that have roles in both guided transport and capture of SVs.

KEYWORDS synaptic vesicle; Sentryn; SAD kinase; Liprin; axonal transport

NEURONS are distinguished from other cells by their complexity. Part of this complexity arises from the need to transport signaling vesicles known as synaptic vesicles (SVs) long distances through axons. Furthermore, after transport, neurons must ensure that SVs become captured in clusters in a specialized *synaptic region*, where synapses form. The synaptic region can be at a nonterminal or a terminal location in the axon, or it can be distributed throughout the axon as part a single process or branched axon processes (Nicholls 2012; Kandel 2013). The captured SVs cluster around small structures known as *active zones*—the sites where SVs ultimately fuse and release their neurotransmitter cargo (Sudhof 2012). Here, we identify what appears to be a new active zone-enriched protein named Sentryn. Our data suggest that Sentryn is a missing link in a sophisticated system that ensures the stable accumulation of SVs at synapses.

The cargo transport system of neurons uses a network of microtubule tracks and motors that exhibit intrinsic directionality. The microtubules have a plus and a minus end, and there are dedicated plus- and minus-end directed motors. The microtubules in axons are nearly uniformly oriented with their plus-ends pointing out (Burton and Paige 1981; Heidemann *et al.* 1981; Baas and Lin 2011). The plus-end directed (forward) motor KIF1A moves SVs from the cell soma to the synaptic region (Hall and Hedgecock 1991). The minus-end directed (reverse) motor dynein moves them in the opposite direction (Ou *et al.* 2010; Edwards *et al.* 2015b). During transport from the soma to the synaptic region, both the forward and reverse motors act on the same SVs, causing them to reverse direction multiple times en route (Wu *et al.* 2013; Edwards *et al.* 2015b). Although the

doi: https://doi.org/10.1534/genetics.118.301466
Manuscript received November 21, 2017; accepted for publication August 27, 2018.
Available freely online through the author-supported open access option.
Supplemental material available at Figshare: https://doi.org/10.25386/genetics.6965732.
[1]These authors contributed equally to this work.
[2]Corresponding author: Oklahoma Medical Research Foundation, 825 Northeast 13th St., Oklahoma City, OK 73104. E-mail: kmiller2686@gmail.com

significance of this bidirectional transport is unknown, its existence means that neurons must have a mechanism to ensure that KIF1A ultimately dominates, thus allowing optimal levels of SVs to reach the synaptic region. We refer to the process that ensures the dominance of forward transport as "guided transport." Adding complexity, neurons must also have a mechanism to inhibit, block, or equalize the actions of both motors after guided axonal transport to enable SVs to become captured in the synaptic region. In other words, SVs must be protected from counter-productive motor activity both during and after transport.

The core synapse stability (CSS) system contributes to both the guided SV transport and the capture of SVs in the synaptic region. The CSS system is a group of proteins with shared functions in inhibiting the removal of cargos from axons (Edwards *et al.* 2015a; Miller 2017). The system includes at least three active zone-enriched proteins, SYD-2 (Liprin-α), SAD kinase, and SYD-1. Despite being enriched at active zones, CSS system proteins also affect transport at sites far removed from active zones, since they guide the outward transport of SVs (Miller *et al.* 2005; Wagner *et al.* 2009; Zheng *et al.* 2014; Edwards *et al.* 2015b). However, the same three proteins also have a post-transport function in the synaptic region near active zones. The synaptic region functions of SYD-2 (Liprin-α), SAD kinase, and SYD-1 were first discovered in *Caenorhabditis elegans*, when mutant analyses revealed defects in SV cluster formation and synapse assembly (Zhen and Jin 1999; Crump *et al.* 2001; Hallam *et al.* 2002; Dai *et al.* 2006; Patel *et al.* 2006). Later studies suggested that the role of these proteins in synapse assembly involved capturing SVs to clusters (Stigloher *et al.* 2011; Kittelmann *et al.* 2013; Wu *et al.* 2013; Edwards *et al.* 2015b). SYD-2 and SYD-1 also contribute to the structure of active zones, but are not required for active zone formation (Zhen and Jin 1999; Owald *et al.* 2010; Kittelmann *et al.* 2013).

The finding that CSS system proteins act together in the same neurons to regulate both the guided transport and capture of SVs suggests that these two processes may be coordinated or linked in some way, possibly through the regulation of motorized transport by a common set of proteins. However, the mechanism by which SV capture occurs is unknown, and past studies have focused more on a physical anchoring mechanism and less on the regulation of motorized transport. Fine filaments have been observed to interconnect SVs in electron tomograms and appear to anchor SVs directly or indirectly to the active zone (Landis *et al.* 1988; Siksou *et al.* 2007; Fernandez-Busnadiego *et al.* 2010; Stigloher *et al.* 2011). However, it is unclear whether the fine filaments serve mainly to protect SVs from diffusion or whether they are also sufficient to protect SVs from the strong forces of motors. Indeed, two recent studies in mice found that dual elimination of either RIM plus RIM-binding protein or ELKS plus RIM led to disassembly of the active zone/dense projection (DP) and eliminated clustering and priming (*i.e.*, docking) of SVs (Acuna *et al.* 2016; Wang *et al.* 2016). However, in those double mutants, wild-type numbers of SVs were still captured at synapses (Acuna *et al.* 2016; Wang *et al.* 2016). This suggests that a capture mechanism not based on physical anchoring, such as motorized transport regulation, may significantly contribute to the captured state. Tethering may act primarily to reduce diffusion of SVs, as has been hypothesized (Landis *et al.* 1988), while motorized transport regulation may protect SVs from the strong forces of motors.

CSS system proteins can also inhibit the dynein-mediated clearance of lysosomes and early endosomes from axons, and can prevent lysosome accumulation in dendrites (Edwards *et al.* 2015a). However, this only occurs in genetic backgrounds lacking UNC-16 (JIP3). JIP3 is a large protein that appears conserved in all animals and that seems to have dual, mostly independent, functions as both a kinesin-1 adaptor and as a regulator of dynein's organelle clearance function in axons (Miller 2017). The combined data from mice, zebrafish, and *C. elegans* suggest that, in the absence of JIP3, the CSS system gains access to lysosomes and early endosomes, and inhibits their dynein-mediated clearance from axons (Miller 2017). The finding that the CSS system can, if given the opportunity, affect the transport of organelles was significant, because it suggests that the CSS system can regulate a cargo transport system that is shared by some organelles as well as SVs. It also provided further evidence that the CSS system can affect transport throughout the neuron, including in dendrites and early segments of the axon, and not just at its sites of enrichment.

Recently, evidence has emerged that the CSS system also regulates the transport and capture of dense core vesicles (DCVs). DCVs mediate the regulated secretion of neuropeptides (Sossin and Scheller 1991; Levitan 2008). Unlike SVs, DCVs are not clustered around active zones, nor are they clustered tightly together with each other in the synaptic region (Weimer *et al.* 2006; Hammarlund *et al.* 2008; Hoover *et al.* 2014). Two separate studies found that *C. elegans syd-2* null mutants accumulate DCVs in cell somas and dendrites in a dynein-dependent manner and have reduced DCV levels in axons (Goodwin and Juo 2013; Edwards *et al.* 2015b). Despite not appearing to have a special relationship with active zones, DCVs were recently found to use the active zone-enriched CSS system proteins SAD kinase and SYD-2 (Liprin-α) for both guided transport and for capture, with DCV capture occurring in the same synaptic region as SV capture (Morrison *et al.* 2018). That study was the first identification of DCV capture proteins. The same study also discovered a role for a novel protein in DCV guided transport and capture. The new protein, which is conserved in all animals, was named *Sentryn*. Based on "sentry," the name is a metaphor for its role in "standing guard" over captured DCVs and "protecting" them from counter-productive motor activity, both during transport and after capture.

Although Sentryn acts with known CSS system proteins in the guided transport and capture of DCVs (Morrison *et al.* 2018), it is unclear whether Sentryn is merely an adaptor that connects the CSS system specifically to the regulation

of DCV motorized transport, or whether it is a new essential component of the CSS system in all contexts. In the current study, we show that, in most contexts, Sentryn is a component of the CSS system. Adding significance, Sentryn appears to be a new active zone protein, suggesting that it the first novel, conserved active zone protein to be discovered in over 11 years. We further show that both Sentryn and SAD kinase, like Liprin-α, contribute to the structure of the active zone, and that Sentryn is recruited to active zones by a process dependent on the active zone protein SYD-2 (Liprin-α). Finally, we show that CSS system proteins are functionally distinct from most other active zone proteins.

Materials and Methods

C. elegans culture and strains

Worm culture and manipulation essentially followed previously described methods (Brenner 1974; Sulston and Hodgkin 1988; Stiernagle 2006). Briefly, culture media was modified NGM (referred to as NGM-LOB) (Hoover *et al.* 2014). Prior studies defined the culture plate types "spread plates," "streak plates," "locomotion plates," "24-well plates," and "96-well solid media culture plates" (Miller *et al.* 1999; Edwards *et al.* 2008, 2015b). "96-well thrashing plates" were made similar to "96-well solid media culture plates" (Edwards *et al.* 2015b) except the media volume per well was 305 μl, and the wells were not seeded with bacteria. The "5 ml unseeded plates" were made by dispensing 5 ml of modified NGM into standard 60-mm Petri plates, allowing them to set overnight at room temperature lid-side-up, and storing unseeded at 4° until needed. The nonwild-type strains used in this study are listed in Supplemental Material, Table S1 in File S1. The relevant mutations present in the worm strains, along with the methods we used for genotyping them in crosses, are listed in Table S2 in File S1.

Targeted knockout of rimb-1 by CRISPR

We inserted the sequence GC TAG C TAA A TGA after codon 16 of the *rimb-1* gene (out of 1276 codons total). The underlined sequence is a *Nhe*I site for snip-PCR screening (Paix *et al.* 2014). The insert contains three stop codons, each in a different reading frame (Paix *et al.* 2014). We used the oligonucleotide-templated coconversion strategy (Arribere *et al.* 2014), using *dpy-10*(*cn64*) as a coconversion marker, and screened for conversion by PCR followed by restriction digest.

We cloned the Cas9 target sequence CATGCCATAGGAGG ATGCGG into the pJP118 gRNA expression cassette as previously described for cloning targeting sequences into pRB1017 (Arribere *et al.* 2014). pJP118 is a modified version of the published pRB1017 plasmid (Arribere *et al.* 2014). It contains a modified sgRNA (F + E), with an extended Cas9 binding structure and removes a potential Pol III terminator by an A–U base pair flip. The oligo template contained 50 bases of homology on each side of this insertion for 113 bases total. The oligo was ordered from Sigma at the 0.2 μmol scale with PAGE purification. The injection mixture was pDD162 (Cas9 plasmid; 50 ng/μl) (Dickinson *et al.* 2013), pJA58 (*dpy-10* gRNA plasmid; 25 ng/μl) (Arribere *et al.* 2014), KG#843 (*rimb-1* gRNA plasmid; 25 ng/μl), and the *dpy-10*(*cn64*) and *rimb-1*(*ce828*) oligo templates (500 and 2400 nM, respectively). We injected 36 wild-type animals with this mixture and cloned 48 F1 rollers, 47 of which yielded progeny. Of the 47 rollers, 34 (72%) showed successful edits, as indicated by *Nhe*I cleavage of a PCR product containing the insertion site.

Plasmids

Table S4 in File S1 lists all the plasmids used in this study along with sources and/or construction details. For the Gibson Assembly plasmid construction using NEBuilder, we followed the manufacturer's instructions with the following options and modifications: (1) we designed primers with 30 bp of overlap, with all of the overlap on one of the two fragments to be combined; (2) we used 15 ng/μl as a starting template concentration for all PCR reactions, rather than the much lower concentration recommended by the manufacturer; (3) we performed the optional *Dpn*I digestions, gel-purified the PCR fragments, and quantified them with a Nanodrop; (4) the assembly reaction contained 200 ng of the vector fragment and a threefold molar excess of each remaining fragment; (5) each reaction was performed in 10 μl total volume, starting with 5 μl frozen aliquots of 2× NEBuilder master mix; and (6) we directly transformed 2 μl of the reaction using electroporation. In all constructs involving the cloning of PCR fragments, we sequenced the inserts and used clones containing no mutations in the fragment of interest to make the final stock.

Production and integration of transgenes

We prepared plasmids for microinjection using the Qiagen Tip-20 system according to the manufacturer's instructions, except that we added a 0.1 M potassium acetate/two volumes ethanol precipitation step after resuspending the isopropanol-precipitated pellet. We produced transgenic strains bearing extrachromosomal arrays by the method of Mello *et al.* (1991). For the *strn-1*(*ok2975*) and *strn-1*(*ok296*) rescue experiments for SV distribution phenotypes, the hosts were KG4787 *strn-1*(*ok2975*); *wyIs85* and KG4943 *strn-1* (*ok2996*); *wyIs85*, respectively. For the *strn-1*(*ok2975*) rescue experiments for lysosome distribution phenotypes, the host was KG4750 *unc-16*(*ce483*); *strn-1*(*ok2975*) *ceIs56*. For all other injection experiments, N2 was the host. We used pBluescript carrier DNA to bring the final concentration of DNA in each injection mixture to 165–175 ng/μl. We integrated transgenes into the genome using 9100 Rads of gamma rays and screening for 100% transmittance of the cotransformation marker as described (Reynolds *et al.* 2005; Charlie *et al.* 2006). We mapped the insertion site of *ceIs259* by crossing the integrant through CB4856, reisolating and cloning homozygous animals in the F2 generation, and

using the resulting mapping lines to map the integration sites relative to SNPs as described (Schade *et al.* 2005). Table S3 in File S1 lists all the transgenes in this study, their DNA contents, and the injection concentration of each DNA.

Strain constructions

We constructed strains containing multiple mutations or transgenes using standard genetic methods (Edwards *et al.* 2015a,b). After making a strain composed of two or more mutations, or one or more mutations plus an integrated transgenic array insertion or an extrachromosomal array, we confirmed the homozygosity of each mutation using the genotyping methods described in Table S2 in File S1.

Light level imaging

File S1 describes the methods used for growth and mounting of strains for imaging, image acquisition and processing, quantitative image analysis, special imaging methods, and immunostaining of formaldehyde-fixed animals.

High-pressure freezing electron microscopy

Worms were prepared using high-pressure freeze (HPF) fixation as described previously (Weimer 2006). Briefly, young adult hermaphrodites were placed in specimen chambers filled with *Escherichia coli* and frozen at −180° and high pressure using a Leica SPF HPM 100. Freeze substitution was then performed on the frozen samples using a Leica Reichert AFS. Samples were held at −90° for 107 hr with 0.1% tannic acid and 2% OsO_4 in anhydrous acetone. The temperature was increased at 5°/hr to −20°, kept at −20° for 14 hr, and increased by 10°/hr to 20°. After fixation, samples were infiltrated with 50% Epon/acetone for 4 hr, 90% Epon/acetone for 18 hr, and 100% Epon for 5 hr. Finally, samples were embedded in Epon and incubated for 48 hr at 65°. All specimens were prepared in the same fixation and subsequently blinded for genotype. Ultrathin (40 nm) serial sections were cut using a Leica Ultracut 6 and collected on formvar-covered, carbon-coated copper grids (EMS, FCF2010-Cu). Poststaining was performed using 2.5% aqueous uranyl acetate for 4 min, followed by Reynolds lead citrate for 2 min. Images were acquired starting at the anterior reflex of the gonad using a Jeol JEM-1220 transmission electron microscope operating at 80 kV. Micrographs were collected using a Gatan digital camera at a magnification of 100,000×. Images were taken of cross-sections of the dorsal cord of three animals for each strain. Cholinergic synapses were identified by morphology (White *et al.* 1986). A synapse was defined as a set of serial sections containing a DP and two flanking sections from both sides without DPs. SVs were identified as spherical, light gray structures with an average diameter of ∼30 nm. A SV was considered docked if it contacted the plasma membrane (*e.g.*, distance to plasma membrane = 0 nm). Images were analyzed using NIH ImageJ software and macros provided by the Jorgensen lab. Serial images were aligned using TrakEM2 before annotating organelle structures in ImageJ. Analysis of these structures was performed using MATLAB scripts written by the Jorgensen laboratory and Ricardo Fleury.

Behavioral analysis

We performed swimming cycle assays using a modification of the originally described "Thrashing Assay" (Miller *et al.* 1996). To grow animals for the assay, we transferred 13 L2 stage larvae to each of four Locomotion Plates and cultured the plates at 20° for 5 2/3 days to produce F1 young adults that had never been starved. The day before the assay, we adjusted the assay area temperature to 22.5–23.5° and set the following items in this area: one "96-well thrashing assay plate" (see "*C. elegans Culture and Strains*"), three "5 ml unseeded plate" (see "*C. elegans Culture and Strains*"), a 2 liter bottle of M9 with a 10 ml bottle top dispenser (set on 6 ml), a 100 ml bottle of M9, a count-down timer set on 3:00 min, a tally counter, and a 2.5 ml Combi-tip attached to a repeat pipetter and set on 75 μl. We made a "25 μl glass pipet tip" by scoring and breaking off ∼4 cm from the end of a Pasteur pipet, inserting a plastic gel-loading tip into the broken end, and securing the junction with Parafilm.

Prior to, and during, the assay, room thermostats were adjusted to keep the assay area temperature at 22.5–23.5°, as monitored by a CheckTemp digital thermometer kept near the stereoscope stage. To start the assay, one of the source plates was transferred from the 20° incubator to the assay area. A 2.5 ml Combi-tip on a repeat pipetter was used to fill the first 12 wells in row A of the 96-well Thrashing Plate with 75 μl of M9. The 5 ml Unseeded Plate was then filled with 12 ml of M9 using the bottle top dispenser; 12 young adult animals were transferred from the source plate into the 12 ml of M9 in the unseeded plate. We then used a P20 set on 25 μl and the 25 μl glass pipet tip to transfer those animals one at a time, in a full 25 μl of M9 to the first 12 wells of the assay plate. We then immediately focused on the animal in the first well, started a count-down timer, and used a tally counter to count swimming cycles for 3 min. We then recorded the counter value on the datasheet, reset the timer and tally counter, focused on the animal in the next well, started the timer, and counted for 3 min, *etc*. until we had assayed all 12 animals. We then repeated this for two more sets of 12 animals for 36 animals total, using a fresh 5 ml unseeded plate for every 24 animals assayed.

When counting swimming cycles, we focused on one side of the animal in the middle of the body and count each time that part goes through a complete cycle. We started the timer when the animal was beginning the cycle, such that the first count represents one complete cycle.

Statistical analysis

We performed most statistical comparisons using the unpaired *t*-test, Welch corrected (for comparisons between two selected groups) or ANOVA followed by the Tukey Kramer post-test (for comparisons involving three or more groups) using Graphpad Instat 3 (Graphpad Software). To compare overall SV distributions relative to the DP (Figure

8), we used the Mann Whitney test on the binned data (run as nonparametric without assuming a Gaussian distribution). All statistical parameters, including the exact value of *n*, what *n* represents, and what error bars represent are reported in the figure legends or in the text for data presented in text form. Throughout the paper, the use of the word "significant" when describing a quantitative result means "statistically significant" ($P < 0.05$).

Data availability

Strains and plasmids are available upon request from the corresponding author, from the *Caenorhabditis* Genetics Center, or from AddGene. The authors affirm that all data necessary for confirming the conclusions of the article are present within the article, figures, and tables. Supplemental files available at FigShare. File S1 contains Figures S1–S6, Tables S1–S4, Supplemental Materials and Methods and Supplemental Material References. Supplemental material available at Figshare: https://doi.org/10.25386/genetics.6965732.

Results

Sentryn acts cell autonomously with CSS system proteins to inhibit the dynein-dependent accumulation of lysosomes in dendrites

In a genetic background lacking UNC-16 (JIP3), CSS system proteins have a property, unique among known proteins, of inhibiting the accumulation of lysosomes in dendrites (Edwards *et al.* 2015a) (see also *Introduction*). If Sentryn is a new CSS system protein, it might be expected to share this activity. To test this, we quantitatively imaged lysosomes in the dendrites of single, identified cholinergic motor neurons in *C. elegans* mutants lacking UNC-16 (JIP3) and in double mutants lacking both JIP3 and Sentryn. In *C. elegans*, Sentryn is also known by the gene name *strn-1* (C16E9.2) or the protein name STRN-1. Throughout this study, we used the null deletion mutants *strn-1*(*ok2996*) and *strn-1*(*ok2975*) (Morrison *et al.* 2018). To visualize individual lysosomes in neurons, we crossed mutants with a genomically integrated transgene that expresses fluorescently tagged lysosomes in a set of nine cholinergic motor neurons (Edwards *et al.* 2013, 2015a).

Two combinations of *unc-16*; *strn-1* double mutants accumulated significantly high numbers of lysosomes in dendrites, ~3.5-fold higher than *unc-16* single mutants (Figure 1A). This phenotype is caused by Sentryn acting cell-autonomously in cholinergic motor neurons because expressing a wild type *strn-1* cDNA in the same neurons rescued dendritic lysosome levels back to the *unc-16* single mutant level (Figure 1A). Sentryn's ability to inhibit lysosome movements into dendrites has been evolutionarily conserved from worms to humans because a human Sentryn cDNA also significantly rescued the worm *strn-1* mutant (Figure 1A).

In a *strn-1* single mutant background (*i.e.*, in a background containing wild-type UNC-16), the lysosome distribution in axons, dendrites, and somas resembled wild type (Figure S1, A–C), although dendritic lysosome levels approached significantly high levels ($P = 0.0507$) (Figure S1B). This is similar to other CSS system single mutants, which also have wild-type, or slightly high, dendritic lysosome levels (Edwards *et al.* 2015a).

The accumulation of lysosomes in *unc-16*; *strn-1* double mutant dendrites correlated with a mild, but significant, reduction of lysosome levels in the cell soma. This could be rescued to *unc-16* single mutant levels by expressing the worm *strn-1* cDNA in the same cells (Figure S2A).

In the *C. elegans* motor neurons we imaged, microtubules in dendrites are oriented primarily with their minus-ends out (Goodwin *et al.* 2012; Yan *et al.* 2013). In mutants lacking both UNC-16 (JIP3) and the CSS system, the dendritic lysosome accumulation is dependent on the minus end-directed motor dynein (Edwards *et al.* 2015a). Although dynein null mutants are sterile in *C. elegans*, a prior study found that the deletion allele *nud-2*(*ok949*) strongly reduces minus-end directed motor activity on SVs in *C. elegans* motor neurons to an extent indistinguishable from strong loss-of-function mutations in DHC-1 (dynein heavy chain) (Ou *et al.* 2010). If Sentryn is a CSS system protein, then the dendritic lysosome accumulation in *unc-16*; *strn-1* mutants should also be dynein-dependent, and, indeed, we found that was the case (Figure 1A and Figure S2A).

If Sentryn functions in the CSS system to inhibit dendritic lysosome accumulation in mutants lacking UNC-16 (JIP3), then combining a *strn-1* null mutation with null mutations in CSS system proteins should not further increase dendritic lysosome accumulation. In an *unc-16*(−) background, the dendritic lysosome levels of a *strn-1* null mutant were not significantly different from null mutants in the CSS system proteins SAD-1 (SAD kinase) and SYD-2 (Liprin-α). The dendritic lysosome accumulation of the *unc-16 sad-1 strn-1* triple mutant was not significantly different from the *unc-16 sad-1* double mutant, while the *unc-16 syd-2 strn-1* triple showed only a small significant increase over the *unc-16 syd-2* double (Figure 1B). Taken together with the results demonstrating dynein-dependence, these results suggest that, for regulating lysosome transport into dendrites in an *unc-16*(−) background, Sentryn's function largely overlaps with the CSS system proteins SAD-1 (SAD kinase) and SYD-2 (Liprin-α).

In unc-16 mutant axons, SAD-1 (SAD kinase) can largely compensate for lack of sentryn

In wild-type axons, UNC-16 (JIP3) is very efficient at ensuring that dynein sends lysosomes back to the soma before they make it out of the axon initial segment (Edwards *et al.* 2013). In axons lacking UNC-16 (JIP3), lysosomes move deeper into the axon and accumulate in the synaptic region (Edwards *et al.* 2013). In the absence of UNC-16 (JIP3), CSS system proteins inhibit the clearance of lysosomes from axons (Edwards *et al.* 2015a). Knocking out the CSS system protein SAD-1 (SAD kinase) reduces the lysosome accumulation in *unc-16* mutant axons by over 80% (Edwards *et al.* 2015a) (Figure 2).

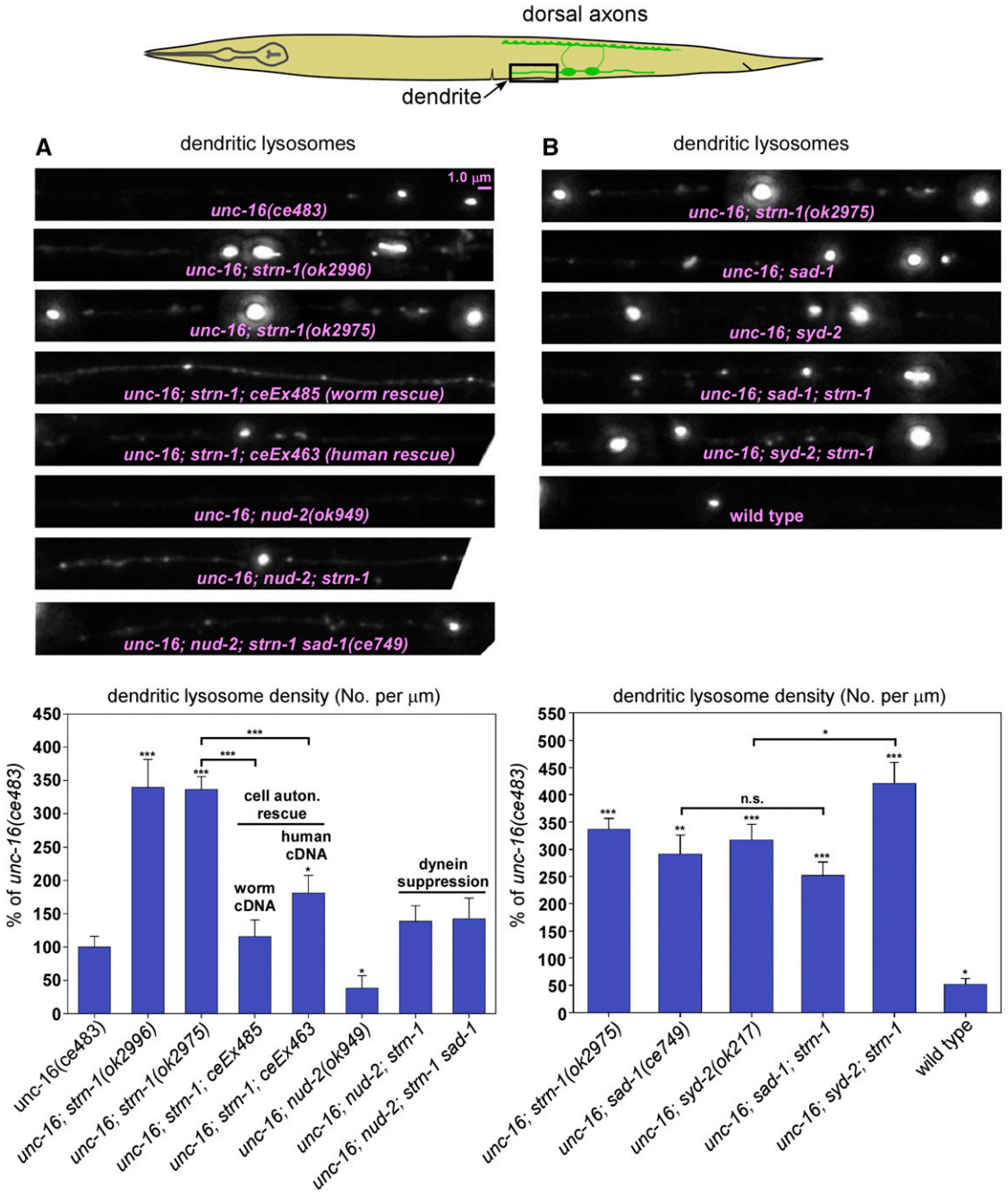

Figure 1 In *unc-16* mutant dendrites, Sentryn acts cell autonomously with the CSS proteins SAD-1 and SYD-2 to inhibit the dynein-dependent accumulation of lysosomes. (A and B) Rectangles in drawing indicate regions imaged. Representative images and quantification of lysosome density in DB6/DA6 dendrites in the indicated genotypes. Where not specified, the *strn-1* allele is *ok2975*. The lysosome marker CTNS-1-RFP is expressed from the integrated transgene *ceIs56*. Representative images are identically scaled. We quantified lysosome density by both number per micrometer and fluorescence intensity per micrometer and obtained similar results. Representative images were chosen based on intensity per micrometer, and the graph data depicts number per micrometer. Graph data are means and SE from 14–15 animals each. Unmarked bars are not significantly different from *unc-16*(*ce483*). *, **, and *** indicate *P*-values that are <0.05, <0.01, or <0.001, respectively. Asterisks that are not above relationship bars compare the indicated bar to *unc-16*(*ce483*).

When we quantified axonal lysosomes in two null alleles of *strn-1* in an *unc-16*(−) background, the reductions were only 20–30%, and this was only significant for one of the two alleles (Figure 2). Furthermore, in quantitative experiments, we did not observe any improvement in locomotion rate for *unc-16*; *strn-1* doubles compared to *unc-16* singles (data not shown) in contrast to the improved locomotion rates of *unc-16*; *sad-1* doubles (Edwards *et al.* 2015a). Overexpressing a wild-type Sentryn cDNA in the same neurons significantly increased, by around twofold, lysosome accumulation in

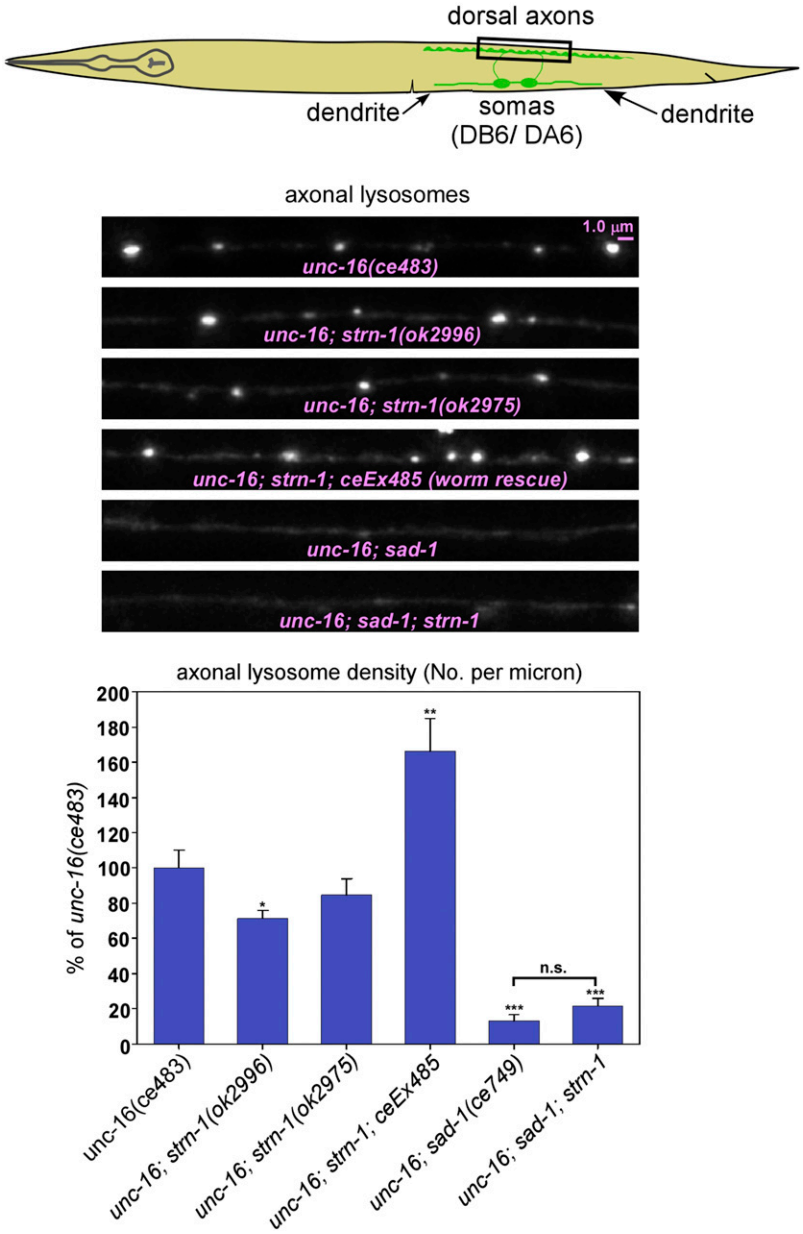

Figure 2 In *unc-16* mutant axons, SAD-1 (SAD kinase) can largely compensate for lack of Sentryn. Rectangle in drawing indicates regions imaged. Representative images and quantification of lysosome density in DB6/DA6 axons in the indicated genotypes. Where not specified, the *strn-1* allele used is *ok2975*. The lysosome marker CTNS-1-RFP is expressed from the integrated transgene *ceIs56*. Representative images are identically scaled. We quantified lysosome density by both number per micrometer and fluorescence intensity per micrometer and obtained similar results. Representative images were chosen based on intensity per micrometer, and the graph data depicts number per micrometer. Graph data are means and SE from 14–15 animals each. Unmarked bars are not significantly different from *unc-16*(*ce483*). n.s., *, **, and *** indicate *P*-values that are >0.05, <0.05, <0.01, or <0.001, respectively. Asterisks that are not above relationship bars compare the indicated bar to *unc-16*(*ce483*). See also related Figures S1 and S2.

unc-16 strn-1 double mutant axons (Figure 2). This suggests that Sentryn can inhibit the clearance of lysosomes from *unc-16* mutant axons. The *unc-16 sad-1 strn-1* triple did not have significantly enhanced axonal lysosome clearance compared to the *unc-16 sad-1* double (Figure 2). These experiments suggest that the CSS protein SAD-1 can largely compensate for lack of Sentryn in the clearance of lysosomes from *unc-16* mutant axons, but the reverse is not true.

In unc-16 mutant neurons, sentryn inhibits the minus-end accumulation of early endosomes

In *unc-16* mutant neurons, early endosomes levels are much lower than wild type in dendrites and much higher than wild type in axons (Edwards *et al.* 2013, 2015a). Knocking out CSS system proteins in an *unc-16*(−) background reduces early endosome levels in axons by 40–60% and increases early endosome levels in dendrites by almost fivefold compared to *unc-16* single mutants (Edwards *et al.* 2015a).

Using a genomically integrated transgene that expresses fluorescently tagged early endosomes in a set of nine cholinergic motor neurons (Edwards *et al.* 2013, 2015a), we found that Sentryn, like CSS system proteins, regulates the distribution of early endosomes in neurons. In dendrites, a *strn-1* null mutation significantly increased the accumulation of early endosomes in *unc-16* mutant dendrites by almost fivefold (Figure 3A). Similar to lysosomes, the effect in axons was smaller, but there was still a highly significant reduction of early endosomes in *unc-16 strn-1* double mutant axons compared to *unc-16* single mutants (Figure 3B).

The mutations we analyzed in this experiment are unlikely to have significantly affected the expression of the early endosome marker because our transgene also coexpressed

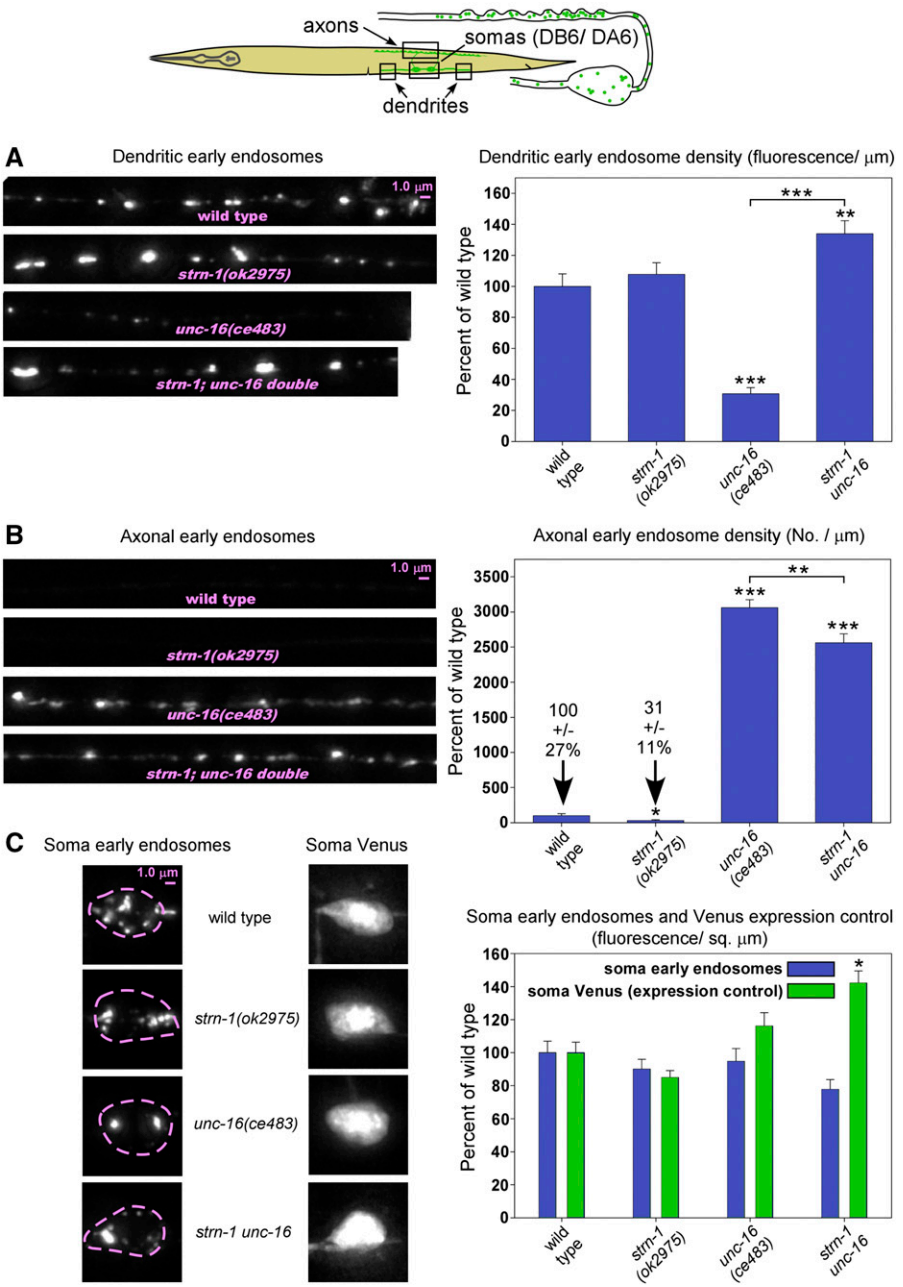

Figure 3 In *unc-16* mutant neurons, Sentryn inhibits the minus-end accumulation of early endosomes. (A–C) Rectangles in the drawing indicate regions imaged. Representative images and quantification of early endosome density in the indicated regions of DA6/DB6 cholinergic motor neurons in the indicated genotypes. The early endosome marker mCherry-SYN-13 is expressed from the integrated transgene *cels259*. Representative images are identically scaled. We quantified endosome density by fluorescence intensity per micrometer in the dendrite and soma (where puncta were more concentrated), and by number per micrometer in the axon. Graph data are means and SE from 14–15 animals each. Unmarked bars in (A and B) are not significantly different from wild type. Unmarked bars in (C) are not significantly different from their corresponding color bar in an *unc-16*(+) background (left 2 strains) or an *unc-16*(−) background (right 2 strains). *, **, and *** indicate *P*-values that are <0.05, <0.01, or <0.001, respectively. Asterisks that are not above relationship bars compare the indicated bar to wild type in (A and B). The asterisk in (C) compares the indicated bar to its corresponding color in the *unc-16*(*ce483*) single mutant group.

soluble YFP under the same promoter as the early endosome marker, and the levels of this coexpressed marker were similar in all strains, with only small changes between strains that would not impact the conclusions of this experiment (Figure 3C).

Sentryn acts with the CSS system proteins SAD-1 and SYD-2 to ensure that optimal levels of SVs accumulate in the synaptic region

To determine if Sentryn, like CSS system proteins, regulates the localization of SVs, we analyzed the distribution of SVs in a single *C. elegans* motor neuron in Sentryn mutants. Using a genomically integrated transgene that expresses a fluorescently tagged SV protein (RAB-3), we found that two independent *strn-1* null mutants had lower densities of SVs in the synaptic region of the DA9 motor neuron when compared to wild type (Figure 4A and Figure S3A). Both mutants also had significantly high levels of SVs in the dendrite, but neither allele had significantly high levels in the cell soma (Figure 4, B–D and Figure S3, B–D). The axonal and dendritic SV distribution phenotypes could be rescued cell-autonomously by expressing a wild type Sentryn cDNA in the DA9 motor neuron (Figure S3, A–D).

To determine if Sentryn acts in the CSS system to regulate SV localization, we analyzed single, double, and triple mutants that included all possible combinations of *strn-1*, *sad-1*, and *syd-2* null mutations. A *sad-1* null mutation reduced SV levels in the synaptic region to a level not significantly different from the *strn-1* null mutant (70–75% of wild type), while

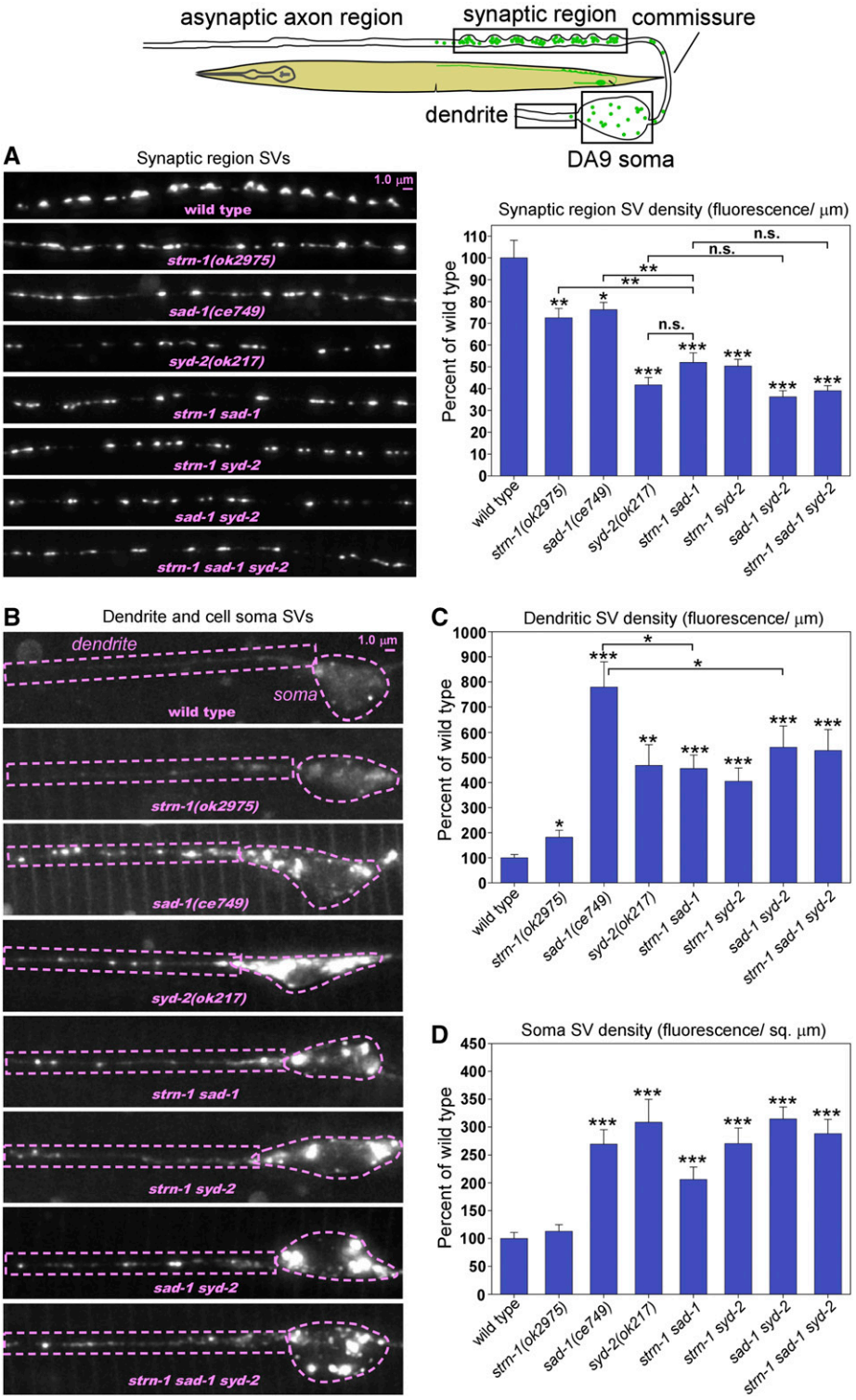

Figure 4 Sentryn acts with the CSS proteins SAD-1 and SYD-2 to ensure that optimal levels of SVs accumulate in the synaptic region. (A–D) Rectangles in the drawing indicate regions imaged. Representative images and quantification of SV density in the indicated regions of the DA9 cholinergic motor neuron in the indicated genotypes. The SV marker GFP-RAB-3 is expressed from the integrated transgene *wyIs85*. Representative images are identically scaled for each region. Dashed lines outline the dendrite and soma regions. Graph data are means and SE from 14–15 animals each. Unmarked bars are not significantly different from wild type. *, **, and *** indicate *P*-values that are <0.05, <0.01, or <0.001, respectively. Asterisks that are not above relationship bars compare the indicated bar to wild type. We also quantified SV levels in the *strn-1* null mutant in the synaptic region of a different motor neuron (DB7) using a different integrated transgene (*cels263*) (Edwards *et al.* 2015b) and got a value similar to that of DA9 (69 ± 5% of wild type; $N = 13$; $P = 0.001$). See also related Figure S3.

a *syd-2* null mutation reduced SV levels in the synaptic region more strongly, to ~40% of wild type (Figure 4A). The *strn-1 sad-1* double was significantly worse than either single mutant, such that its SV density in the synaptic region was not significantly different from the *syd-2* null. However, neither *strn-1 syd-2* nor *sad-1 syd-2* double mutants were significantly different from *syd-2* single mutants. Furthermore, the SV density of the *strn-1 sad-1 syd-2* triple was not significantly worse than the *syd-2* single mutant or the *strn-1 sad-1* double (Figure 4A). This suggests that all three proteins act in the same system. However, in this context, Sentryn and SAD kinase each appear to have at least one nonoverlapping function, and their combined overlapping and nonoverlapping functions together enable the function of SYD-2 (liprin-α).

In the dendrite and soma, wild type has very low levels of SVs. *sad-1* and *syd-2* null mutants have much higher levels of SVs in these regions, while levels in *strn-1* null mutants are significantly higher than wild type, but significantly lower than *sad-1* and *syd-2* mutants (Figure 4, B–D and Figure S3, B–D). No combination of these three mutations resulted in additive effects (Figure 4, B–D). However, in the dendrite, both *sad-1 strn-1* and *sad-1 syd-2* double mutants have significantly lower levels of SVs than *sad-1* single mutants (Figure 4, B–D). Although the reason for this suppression is unclear, the results suggest that all three proteins function in the same system in the context of the soma and dendrite, with Sentryn having a more minor role in the function that determines SV levels in these locations.

Sentryn acts with the CSS proteins SAD-1 and SYD-2 to promote accumulation of SVs in the synaptic region

Previously, we showed that CSS system proteins act to ensure that KIF1A outcompetes dynein during the outward transport of SVs to the synaptic region (Edwards *et al.* 2015b). In CSS system null mutants, KIF1A is no longer able to outcompete dynein to the same extent as it is in wild type, thus causing a fraction of the total SV population to build-up in cell somas and dendrites in a dynein-dependent manner (Edwards *et al.* 2015b).

The accumulation of SVs in somas and dendrites (*i.e.*, defective forward transport of SVs) likely contributes to the lower SV density in the synaptic region of Sentryn and CSS system mutants. This makes sense: if more SVs accumulate in the soma and dendrite, then there might be fewer available to go to, or be retained at, the synaptic region. However, it is possible that a defect in the capture of SVs in the synaptic region also contributes to the lower SV densities in the synaptic region of Sentryn and CSS system mutants. Indeed, for DCVs, which are more amenable to direct visualization of capture and capture defects and use the same transport motors as SVs, both guided transport and capture defects were found to significantly contribute to the altered DCV distributions in the CSS and Sentryn mutants (Morrison *et al.* 2018).

The DA9 motor neuron in *C. elegans* provides an ideal system to assay for SV capture defects because it contains a short, nonterminal synaptic region sandwiched between proximal and distal asynaptic regions (White *et al.* 1986; Klassen and Shen 2007). If a SV or a small cluster of SVs fails to be captured in the synaptic region, motors could theoretically move SVs to either of the flanking asynaptic regions where they would accumulate. To test for SV capture defects in Sentryn and CSS system mutants, we used a large field-of-view camera and multiple, overlapping images to assemble a high-resolution view of fluorescently tagged SVs along the entire 0.5 mm long DA9 axon in wild-type, Sentryn, SAD Kinase, and Liprin-α null mutant adults. We then produced profile plots of the SV distributions in the DA9 axon and measured the length of the region with SV signals exceeding a predefined threshold. In this assay, an expanded length is the expected result for a SV capture defect.

In wild type, SVs were tightly restricted to a 100 μm region and did not accumulate in either of the flanking asynaptic regions (Figure 5A). In a null mutant lacking the CSS system protein SYD-2, SVs were reduced in the synaptic region and accumulated in both flanking asynaptic regions (Figure 5A). Although SVs filled nearly the entire distal asynaptic region of the *syd-2* mutant axon, they were not quite randomly distributed, but still showed an enrichment in the synaptic region. Quantification of the length of the region with SVs revealed an over fourfold expansion in length that, on average, filled most of the axon (Figure 5B).

The *strn-1* single mutant showed a small but significant increase in the length of the region with SVs (hereafter referred to as expansion length) (Figure 5B). The *sad-1* null mutant's expansion length was intermediate between the significantly longer expansion length of the *syd-2* null mutant and the significantly shorter expansion length of the *strn-1* mutant (Figure 5B). The *strn-1 sad-1* double null mutant showed an additive effect, with an expansion length significantly longer than either single mutant and not significantly different from the *syd-2* single mutant (Figure 5B). The *strn-1 syd-2* double mutant was not significantly worse than the *syd-2* single mutant, suggesting that Sentryn acts in the same process as SYD-2 (Liprin-α) in this context. However, the expansion length of the *sad-1 syd-2* double mutant was slightly, but significantly, worse than the *syd-2* single mutant, and the expansion length of the *strn-1 sad-1 syd-2* triple was significantly worse than the *strn-1 sad-1* double (Figure 5B). These latter results suggests that SAD kinase has some capture activity in the absence of SYD-2, and that SYD-2 has a small amount of capture activity in the combined absence of Sentryn and SAD kinase.

Overall, these results suggests that all three proteins act as part of the same system in this context, but that SAD kinase and SYD-2 can also act independently of each other to a small degree. Furthermore, in this context, Sentryn and SAD kinase each appear to have at least one nonoverlapping function, and their combined overlapping and nonoverlapping functions together appear to enable most of the function of SYD-2 (Liprin-α).

SV misaccumulations in asynaptic regions of other neuron types

Misaccumulation of SVs in an asynaptic region may be easier to detect in *C. elegans* ventral cord cholinergic motor neurons than in other neurons due to the presence of their long distal asynaptic regions. These regions, hypothesized to contain stretch receptors (Chalfie and White 1988), provide a large reservoir in which SVs that may have evaded capture at the synaptic region can accumulate. This may also contribute to greater losses of SVs from clusters in the synaptic region than would otherwise be observed. Most neurons lack such an extensive distal asynaptic region. What does SV misaccumulation in asynaptic regions look like in neurons without a long distal asynaptic region? Do CSS system proteins also contribute to localizing SVs to synapses in such neurons?

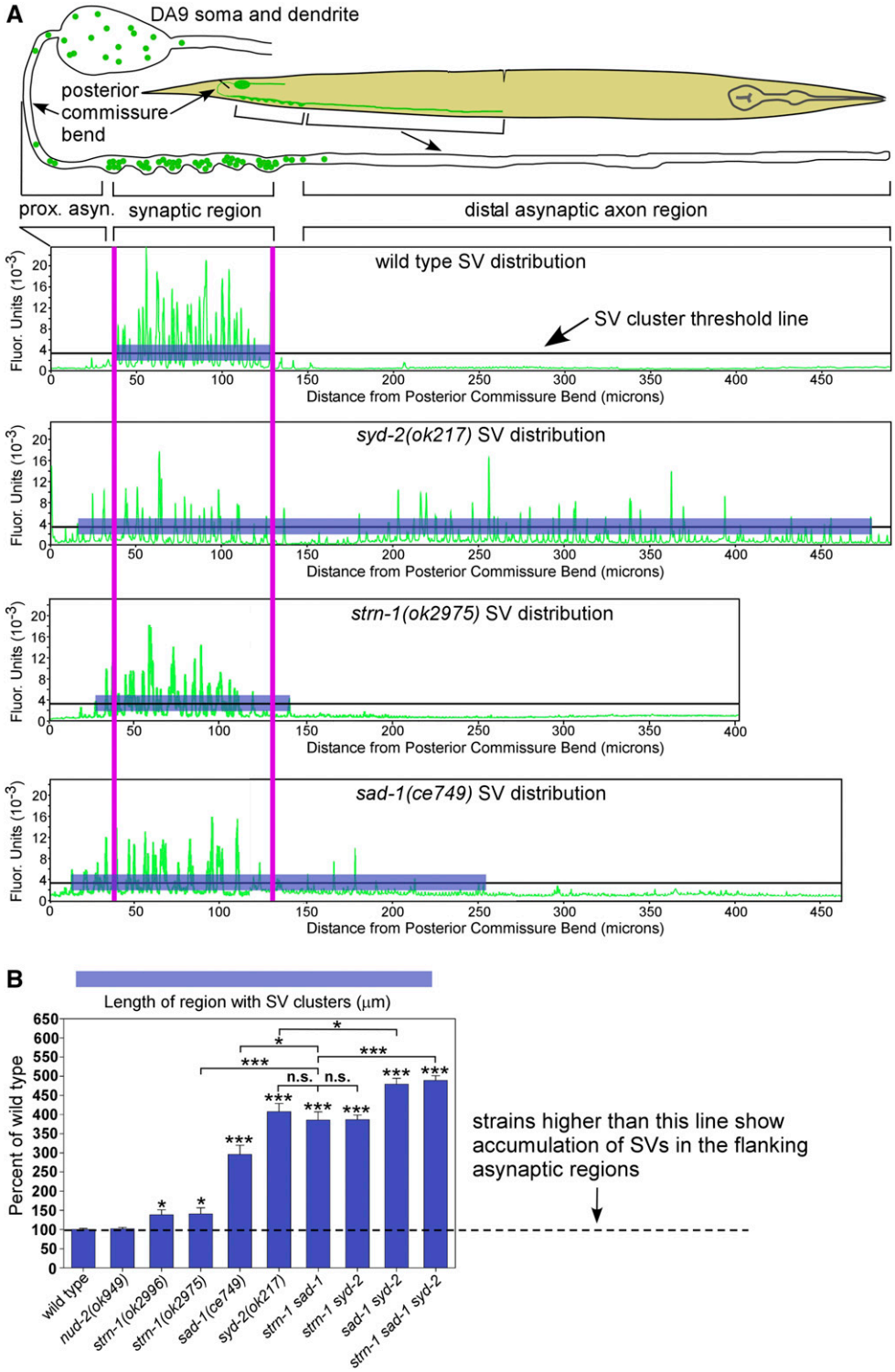

Figure 5 Sentryn acts with the CSS proteins SAD-1 and SYD-2 to promote the capture of SVs in the synaptic region. (A) Drawing indicates regions of the DA9 motor neuron. Graphs plot fluorescence intensity of the SV marker GFP-RAB-3 as a function of distance from the posterior commissure bend for a single representative animal of each indicated genotype. A threshold line indicates the intensity cut-off used for defining SV clusters. Blue highlighted segments indicate regions exceeding the threshold in wild type and the indicated mutants. Pink vertical lines connect identical locations in wild type and the indicated mutants to show that SVs mislocalize both proximal and distal to the synaptic region in the mutants. High resolution images acquired with a large field-of-view Flash 4.0 camera were used to reconstruct the dorsal axon from multiple images. GFP-RAB-3 is expressed from the integrated transgene array *wyIs85*. (B) Graph quantifies SV capture efficiency in the indicated genotypes by measuring the length of the region with SV clusters exceeding the threshold line (shown in A). This quantifies the extent to which SVs have overshot the synaptic region and have moved toward microtubule plus ends in the long asynaptic region or, alternatively, have spread in the minus direction toward the soma. Graph data are means and SE from 14–15 animals each. Where not specified, the *strn-1* allele used is *ok2975*. * and *** indicate *P*-values that are <0.05 or <0.001, respectively. Asterisks that are not associated with relationship bars compare the indicated strain to wild type.

To address these questions, we imaged native SV clusters in the sublateral axons of *C. elegans*. In contrast to the DA9 motor neuron axon, these axons do not have a single defined synaptic region, but instead have relatively widely spaced synapses along their length. Each intersynaptic region in these axons is thus the equivalent of a short asynaptic region. Thus, in mutants that are unable to prevent SVs from escaping the synaptic region, SVs, or microclusters of SVs, should accumulate in the intersynaptic regions.

To test this, we immunostained adult animals using a monoclonal antibody specific for the synaptic vesicle ACh transporter, and then quantitatively imaged SV clusters in the sublateral axons. Wild-type clusters showed the expected pattern of relatively widely spaced prominent clusters with

intersynaptic regions containing few or no SV microclusters. In contrast, mutants lacking Sentryn and/or SAD kinase showed a "broken-up" pattern of microclusters interspersed with larger clusters. The largest clusters in the mutants appeared similar in size to small wild-type clusters (Figure 6, A and B).

Consistent with the predicted accumulation of SV microclusters in intersynaptic regions, *strn-1* and *sad-1* null single mutants had significantly higher numbers of clusters and microclusters per micrometer of axon length (Figure 6C). Although the cluster densities of *strn-1* and *sad-1* single mutants were not significantly different from each other, the *strn-1 sad-1* double mutant had a higher average cluster density than either single mutant (~140% of wild type). This was significant when comparing the double to *strn-1* single mutants, but not quite significant when comparing the double to *sad-1* single mutants (Figure 6C).

If SVs misaccumulate in microclusters in intersynaptic regions, this should not change the total SV content per unit length of the axon. Indeed, that is the result we obtained for *syd-2* null mutants when analyzing the DA9 axon using transgenically tagged SVs (Edwards *et al.* 2015b). Consistent with this, the average SV fluorescence per micrometer of *strn-1* and *sad-1* single mutant axons was not significantly different from wild type, although it trended lower (Figure 6D). The average SV fluorescence per micrometer of the *strn-1 sad-1* double was slightly, but significantly, lower than wild type (~80% of wild type; Figure 6D). Since many microclusters are barely detectable above the high background inherent in any immunostaining experiment, we suggest that the lower level in the *strn-1 sad-1* double results from some fraction of microclusters evading detection due to masking by the background. The likelihood of this occurring should be higher in the *strn-1 sad-1* double than in either single mutant due to the larger number of microclusters in the double, as shown in Figure 6C.

The above analysis of SV clusters in sublateral axons provides an alternative view of SV misaccumulation in asynaptic regions in *sad-1* and *strn-1* mutants that complements the analysis of the DA9 axon. These results also appear to provide independent, complementary evidence suggesting that Sentryn and SAD kinase each have at least one nonoverlapping function consistent with a deficiency in capturing SVs in synaptic regions (*i.e.*, that the double mutant tends to be more severe than either single mutant).

Presynaptic ultrastructure and SV distributions relative to the active zone are significantly altered in mutants lacking sentryn and/or SAD kinase

To determine if the reductions in synaptic region SVs in mutants lacking Sentryn and/or SAD kinase were occurring precisely at synapses, we first quantified native SVs in cholinergic motor neuron synapses using HPF electron microscopy (EM). In all, we sampled an average of 15 synapses taken from a total of three animals each for wild type and strains lacking Sentryn and/or SAD kinase. The results, obtained blinded, closely matched the results we obtained by imaging transgenically tagged SVs in axons, where we sampled a much larger number of synapses (typically a total of ~375 synapses taken from a total of 15 animals per genotype). Wild type synapses, reconstructed from an average of 13 thin (40 nm) sections that spanned each synapse, had an average of 412 SVs (Figure 7A). SVs at *strn-1* and *sad-1* null mutant synapses were reduced to 63 and 72% of wild type, respectively (Figure 7A), similar to the above results for transgenically tagged SVs. Due to the small sample size and high variability of SV numbers between synapses, this was not statistically significant for either mutant. However, SV numbers at *strn-1 sad-1* double mutant synapses were further reduced, to 52 ± 6% of wild type (Figure 7, A and D). This was highly significant and closely matched the above result for transgenically tagged SVs in the same double mutant (*i.e.*, Figure 4A).

Although docked SVs were also significantly reduced in the *sad-1* single mutant and the *strn-1 sad-1* double (Figure 7B), we did not find evidence for a specific defect in SV docking. Instead docked SVs were simply reduced proportional to total SVs (Figure 7B), as was previously found for *syd-2* null mutants (Kittelmann *et al.* 2013). The *strn-1 sad-1* double mutant showed the strongest significant reduction in docked SVs, to 53% of wild type, closely matching the reduction in total SVs (Figure 7B).

A previous study found that the DP, which is the electron dense structure at the center of the active zone, was reduced in length in mutants lacking SYD-2 (Liprin-α) (Kittelmann *et al.* 2013). If Sentryn and SAD kinase have functions that overlap with Liprin-α at the active zone, mutants lacking Sentryn and/or SAD kinase might also show this ultrastructural defect. Indeed, we found that DP length, measured in blinded samples by counting the number of 40 nm sections that contained a single DP, was significantly reduced in all three mutant strains lacking Sentryn and/or SAD kinase (Figure 7C). The strongest, most significant reduction in DP length occurred in *strn-1 sad-1* double mutants (50% of wild type), although its value was not statistically different from either single mutant (Figure 7C).

We next sought to determine the regions of the synapse from which SVs are missing in mutants lacking Sentryn and SAD kinase. Because the DP length is reduced in mutants lacking Sentryn and/or SAD kinase, and because SVs are known to cluster around the DP (Stigloher *et al.* 2011), we hypothesized that the missing SVs in mutants lacking Sentryn and SAD kinase might be those SVs that are closest to the DP, or, alternatively, that SVs might be uniformly reduced regardless of their location relative to the DP. To determine this, we divided synapses into 33 nm wide zones progressively extending from the DP and counted the SVs in each zone. Unexpectedly, the data showed that SVs in mutant synapses lacking Sentryn, or both Sentryn and SAD kinase, were present in wild type numbers in zones that were ≤165 nm from the DP, while SVs in zones farther than 165 nm, specifically 165–700 nm from the DP, were present at lower numbers than wild type (Figure 8, A–C). When individually comparing

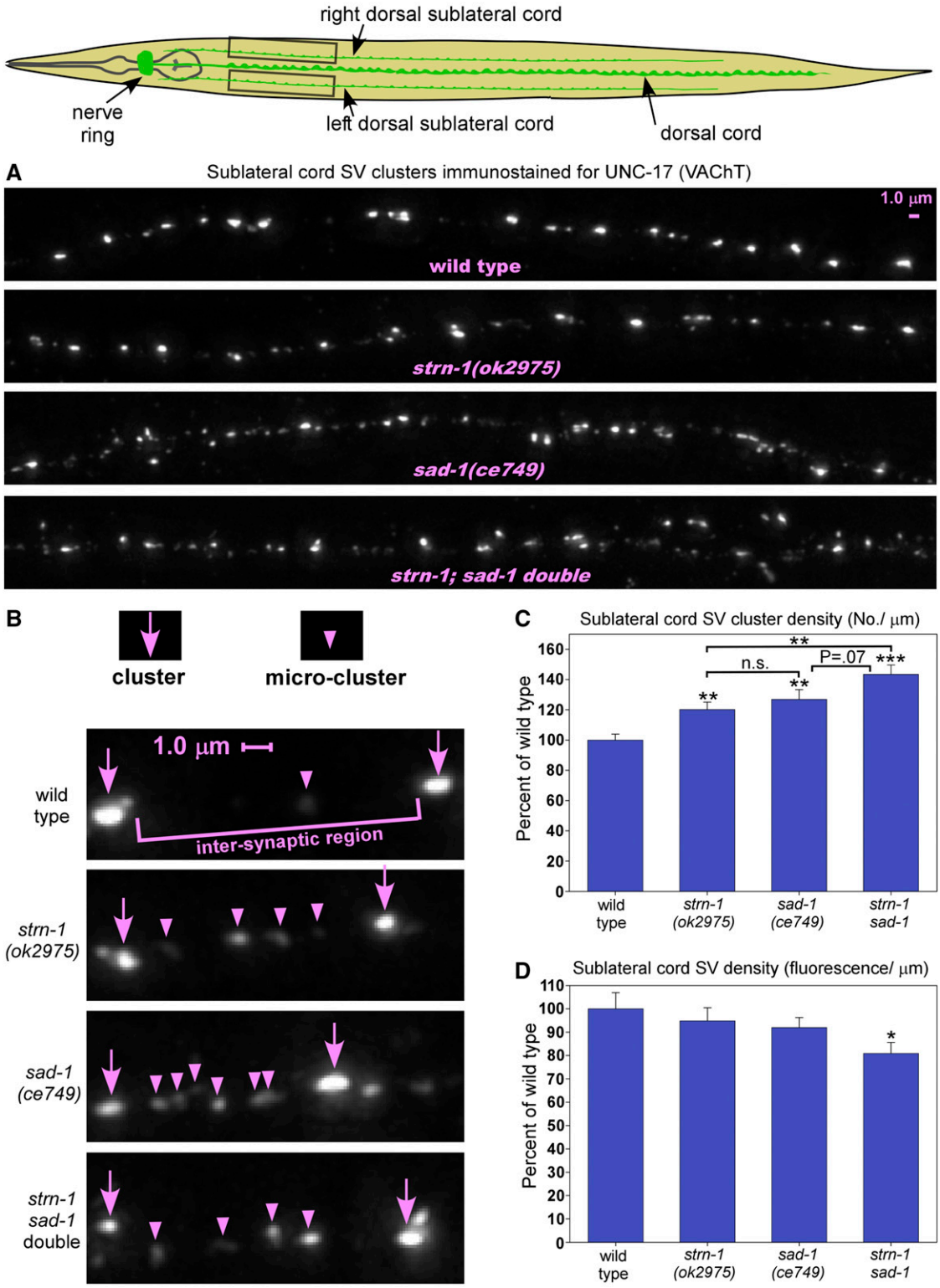

Figure 6 Capture failure in a neuron lacking a long distal asynaptic region. (A) Rectangle in drawing shows regions imaged. Representative, identically scaled images of native UNC-17 (SV ACh transporter) immunostaining in sublateral axons of wild type and mutants lacking Sentryn and/or SAD kinase. (B) Expansion of images from (A) showing the accumulation of microclusters of SVs in the intersynaptic regions between widely spaced larger clusters in mutants lacking Sentryn and/or SAD kinase. (C and D) Quantification of native UNC-17 (SV ACh transporter) immunostaining in sublateral axons of animals with the indicated genotypes. Graphs quantify average cluster number per micrometer of axon length (C) and average fluorescence per micrometer of axon length (D). Data are means and SE from 18 animals each. Unmarked bars are not significantly different from wild type. *, **, and *** indicate *P*-values that are <0.05, <0.01, or <0.001, respectively. Asterisks that are not above relationship bars compare the indicated bar to wild type.

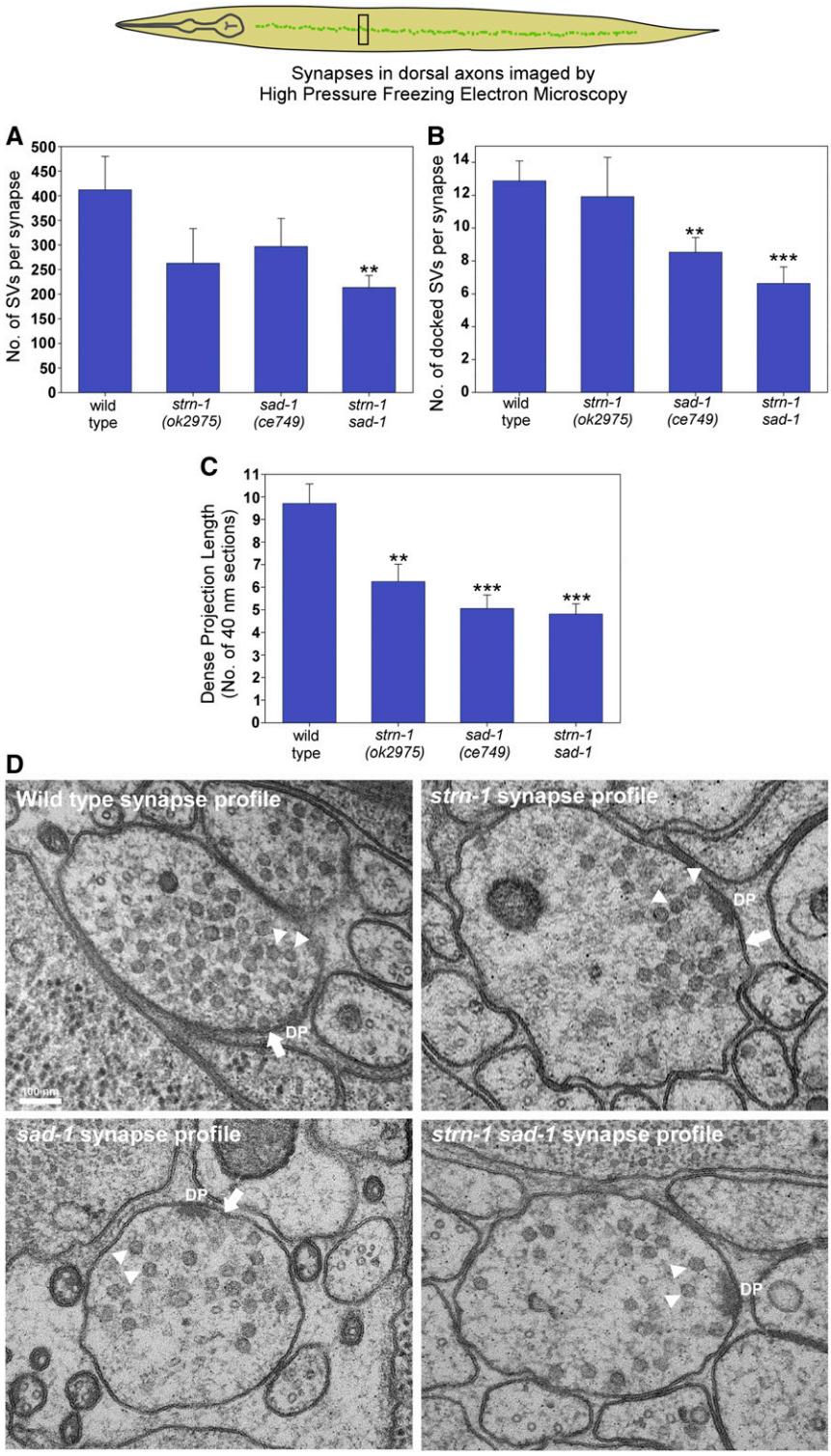

Figure 7 Presynaptic ultrastructure is significantly altered in mutants lacking Sentryn and/or SAD Kinase. Rectangle in drawing shows approximate region imaged. (A–C) Graphs plotting various indicated parameters of presynaptic ultrastructure of cholinergic motor neuron synapses visualized by HPF EM. Graph data are means and SE from 17, 12, 17, to 16 synapses reconstructed from 220, 115, 150, to 134 thin (40 nm) sections for wild type, *strn-1*, *sad-1*, and *strn-1 sad-1* double mutants, respectively. ** and ** indicate *P*-values that are $\leq$0.01 or $<$0.001, respectively. Note that the DP size varies between profile sections. "Dense Projection Length" represents the number of 40 nm cross-sections containing a DP and not the length of the DP in the below single cross-section images (see below). (D) Representative 40 nm single-section images of the indicated genotypes, taken near the center of the DP. Two of the many SVs in each image are indicated with arrowheads, along with the DP. A single docked SV (arrow) is visible in wild type and the single mutants, but not the *strn-1 sad-1* double. Note that each single 40 nm section is only 7–10% of a synapse. The size of the DP in these images of individual sections is not indicative of the overall DP length measured in (C) due to the convoluted bay shape of the DP, which spans many sections.

corresponding zones of each mutant strain to wild type, this reached significance in the Sentryn single mutant for two zones covering ~350–400 nm from the DP and, in the Sentryn/SAD kinase double mutant, for nine zones covering ~250–550 nm (Figure 8, A–C). When comparing the overall SV distributions of wild type to each mutant strain using the Mann-Whitney test, the Sentryn single mutant and the Sentryn/SAD kinase double SV distributions were significantly different from wild type (*i.e.*, significantly skewed such that more distal SVs were missing). The SV distribution of the SAD kinase single mutant trended toward, but did not reach, significance, but all zones in the SAD kinase single mutant >165 nm from the DP had fewer SVs than wild type (Figure 8, A–C).

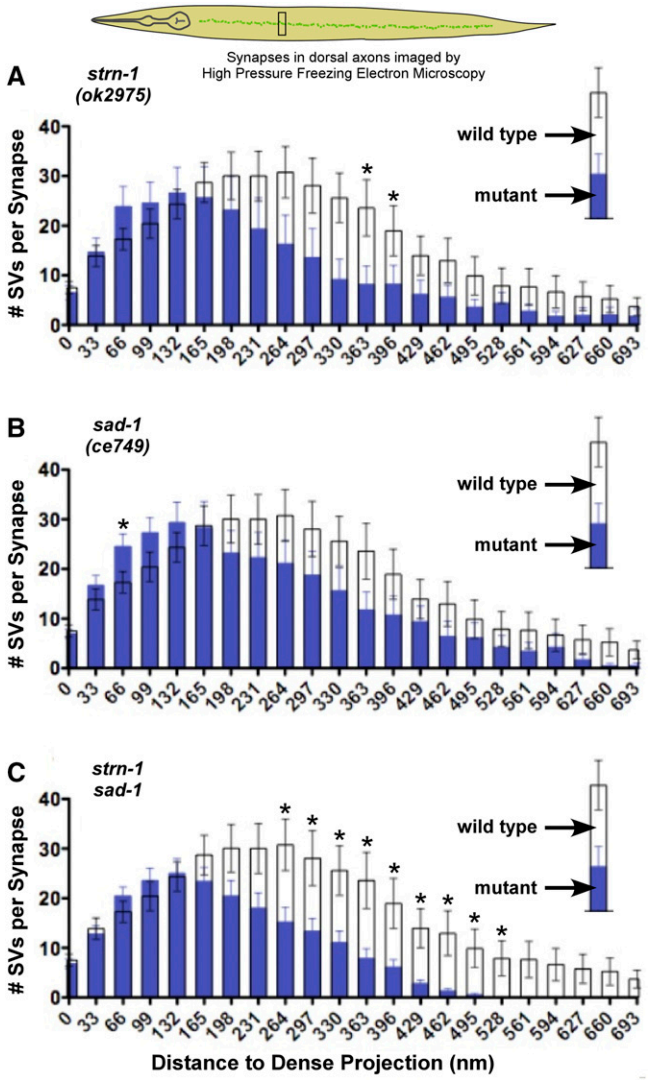

Figure 8 SVs farther than 165 nm from the DP are selectively reduced in mutants lacking Sentryn and/or SAD kinase. Rectangle in drawing shows approximate region imaged. (A–C) Graphs plot the distance of each SV from the DP in the indicated genotypes using a bin size of 33 nm. Unfilled wild type bars are overlaid on each mutant plot to facilitate comparison. Cholinergic motor neuron synapses were visualized by HPF EM. Graph data are means and SE from 17, 12, 17, to 16 synapses reconstructed from 220, 115, 150, to 134 thin (40 nm) sections for wild type, *strn-1*, *sad-1*, and *strn-1 sad-1* double mutants, respectively. The number of SV-to-DP distances analyzed for each strain were 7812, 3282, 5357, and 3616, respectively. * $P < 0.05$ by an unpaired two-tailed *t*-test when comparing corresponding bins of each mutant strain to wild type. Note that the asterisks do not reflect the significance of the overall SV distribution relative to the wild type distribution. The *P* values for comparing the overall distribution of SVs between wild type and each mutant strain are 0.038 (significant), 0.16 (not significant), and 0.011 (significant) for the *strn-1*, *sad-1* and *strn-1 sad-1* mutant strains, respectively, using the Mann Whitney test (run on the binned data as nonparametric without assuming a Gaussian distribution). For representative images see Figure 7D.

Overall, the EM results, though lacking the statistical power of the transgenically tagged SV studies, are consistent with the reductions of SVs at synapses that we observed in the transgenic studies. Furthermore, the EM studies added important new information by identifying the synapse zones in which SVs are missing in mutants lacking Sentryn or both Sentryn and SAD kinase. Finally, the finding that Sentryn contributes to the structure of the active zone in a manner similar to the active zone proteins Liprin-α, which functions in the same pathway as Sentryn, suggests the intriguing possibility that Sentryn could be a new active zone protein.

Sentryn appears to be a new active zone protein that is dependent on another active zone protein for its localization

Active zones, which mark the sites of SV exocytosis, are the focal points around which SVs are captured in the synaptic region (Weimer *et al.* 2006; Stigloher *et al.* 2011; Hoover *et al.* 2014). The CSS system proteins SYD-2 (Liprin-α) and SAD kinase are enriched at active zones (Ackley *et al.* 2005; Yeh *et al.* 2005; Inoue *et al.* 2006; Weimer *et al.* 2006; Fouquet *et al.* 2009). Since the data suggest that Sentryn is also a CSS system protein, and, since the above results show that it plays a role in active zone ultrastructure, we hypothesized that Sentryn might also be enriched at active zones. Our data suggest that is the case. Sentryn largely colocalizes with the active zone-enriched proteins UNC-10 (RIM) and SAD-1 (SAD Kinase) (Figure 9A). When we expressed a rescuing version of full-length GFP-tagged Sentryn at low levels in the DB7 motor neuron, we observed a highly focal localization of Sentryn in a small area of each bouton at the ventral apex of the bouton. The ventral apex is the precise location of the active zone (Figure 9B). In contrast, in a *syd-2* null mutant, Sentryn was present in the synaptic region, but showed a diffuse or patchy diffuse localization and was not enriched at the ventral apex (Figure 9C). In a *sad-1* null mutant, Sentryn's localization appeared partially disrupted, sometimes localizing to the ventral apex and sometimes appearing unlocalized or localizing to bouton regions other than the ventral apex (Figure 9C). In general, Sentryn localization is variable in animals lacking *sad-1*. This is evident when comparing a panel of Sentryn localization images from different *sad-1* mutant animals (Figure S6).

In summary, these data suggest that Sentryn is enriched at active zones, and that Sentryn physically interacts with SYD-2 (Liprin-α), or with a SYD-2-dependent protein or complex, to be recruited to active zones. Furthermore, Sentryn appears partially dependent on SAD kinase for localization to active zones.

CSS system proteins are a specialized set of active zone-enriched proteins with unique roles in ensuring the stable accumulation of SVs in the synaptic region

Given that the three CSS proteins we investigated in this study all appear to be active zone-enriched proteins, we wondered if any other active zone-enriched proteins might also have roles in the stable accumulation of SVs in the synaptic region. Indeed, we previously found that SYD-1 acts in the CSS system, and that *syd-1* null mutants have impaired SV transport

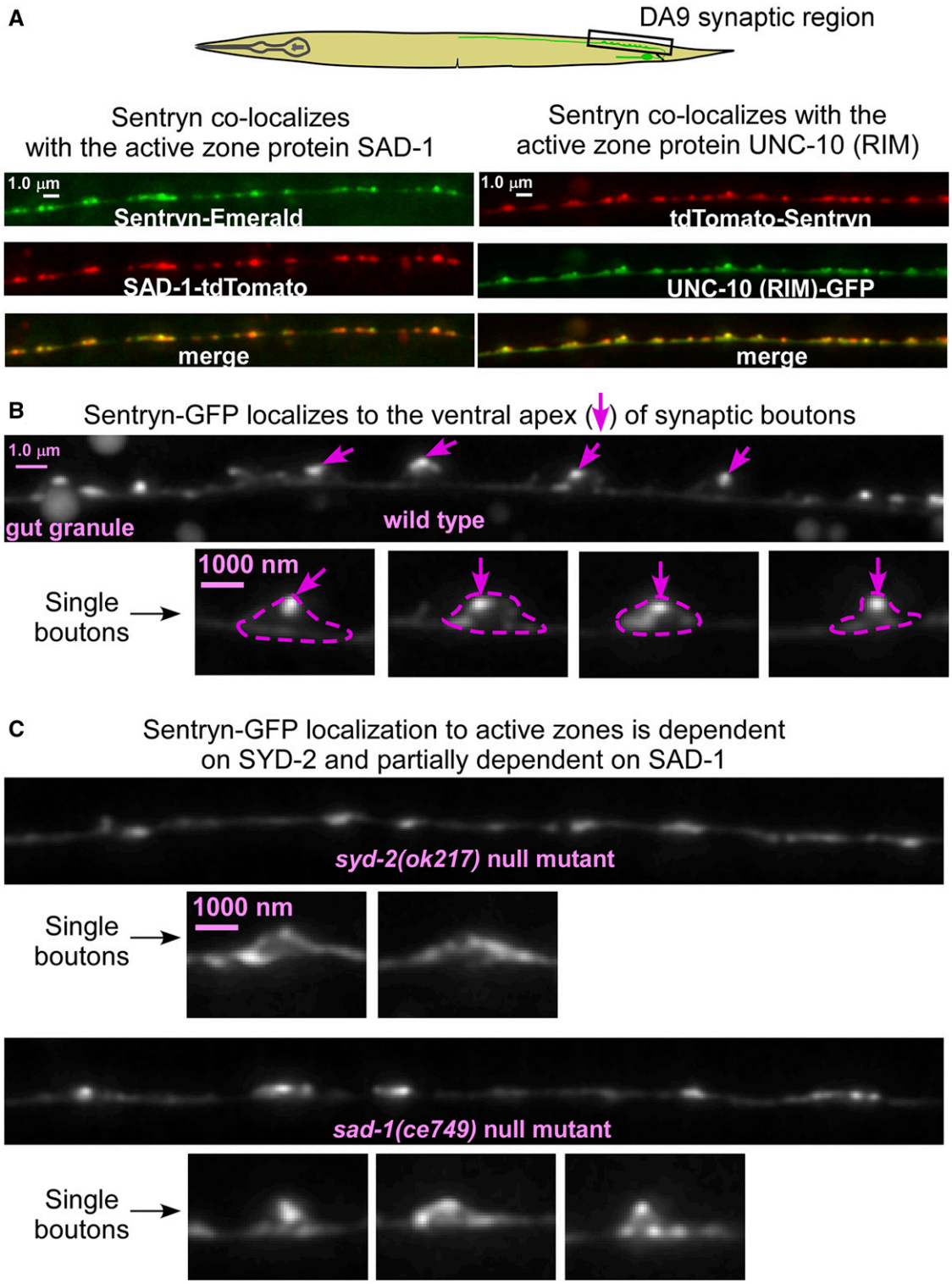

Figure 9 Sentryn shows a SYD-2-dependent enrichment at active zones. [see above]. (A) Rectangle in drawing shows region imaged. Representative images showing colocalization of Sentryn with the active zone proteins SAD-1 and UNC-10 (RIM) in the DA9 motor neuron synaptic region. Sentryn-Emerald and SAD-1-tdTomato are coexpressed from the *ceEx510* transgenic array. tdTomato-Sentryn and UNC-10 [627-974]-GFP are coexpressed from the *ceEx503* transgenic array. (B) Representative images showing localization of Sentryn-GFP to the ventral apex of boutons (the location of the active zone) at DB7 motor neuron synapses. Note the highly focal localization of Sentryn-GFP to the ventral apex as indicated with arrows. Single bouton images (indicated) are from three different animals, and includes two of the boutons enlarged from the multi-bouton image. Dashed lines outline the approximate boundaries of the boutons as determined by the nonfocal Sentryn-GFP signal that fills the bouton at a lower concentration. Sentryn-GFP is expressed from the *ceEx462* transgenic array, and is functional because it restores wild-type function to a *strn-1* null mutant (Figure S4). (C) Representative images showing localization of Sentryn-GFP in the DB7 motor neuron synaptic region in the indicated mutant backgrounds. The single- and

and SV capture in the synaptic region (Edwards *et al.* 2015a,b). SYD-1 is an active zone-enriched protein with PDZ, C2 and rhoGAP-like domains (Hallam *et al.* 2002; Owald *et al.* 2010), and it also functions with SYD-2 (Liprin-α) and SAD-1 (SAD kinase) in synapse assembly in *C. elegans* (Dai *et al.* 2006; Patel *et al.* 2006). Could other active zone-enriched proteins also have roles in ensuring the stable accumulation of SVs in the synaptic region?

To test this, we analyzed putative null mutants in seven other active zone-enriched proteins using our capture failure assay in the DA9 motor neuron (*i.e.*, the assay used for Figure 5). One of the mutants, the *rimb-1* (rim-binding protein) null mutant, showed a slight (<10%), but significant, expansion of SVs into the flanking asynaptic regions (Figure S5, A and B). Consistent with RIMB-1 having a role in the CSS system, SVs also accumulated in *rimb-1* mutant dendrites (192 ± 32% compared to wild type; $N = 15$; $P = 0.015$; Figure S5D). However, unlike other CSS system mutants, the overall density of SVs in the DA9 synaptic region of the *rimb-1* null mutant was not significantly reduced (103 ± 4% of wild type, $N = 15$; Figure S5C). None of the other six mutants showed significant SV accumulation outside of the synaptic region (Figure S5B). These mutants included null mutants in UNC-13 and five active-zone-enriched proteins known to interact with SYD-2 (see Figure S5B for protein names and references). Indeed, null mutants lacking UNC-10 (RIM) or UNC-13 showed a small but significant compression of the synaptic region (∼80% of wild type; Figure S5B). Thus, with the possible exception of a minor or redundant role for RIMB in the CSS system, none of the other six active zone proteins we tested have essential roles in the SV capture function of the CSS system in *C. elegans*.

Sentryn mutations impair locomotion behavior

The release of ACh from SVs at ventral cord motor neuron synapses is essential for locomotion (Alfonso *et al.* 1993). To determine if Sentryn and/or SAD kinase contribute to locomotion behavior, we quantified the rate of swimming cycles in wild type and mutants lacking Sentryn and/or SAD kinase. Placing *C. elegans* in liquid over a smooth agar surface induces an escape response, in which the animal alters its locomotion pattern and attempts to escape the liquid via high frequency swimming cycles. We counted swimming cycles in at least 36 wild-type and mutant animals for 3 min per animal and obtained averages. At 23°, wild type has ∼100 swimming cycles per minute (Figure 10). Two mutants putatively null for Sentryn swam at a rates significantly lower than wild type (74% and 85%, respectively), while the *sad-1*(*ce749*) mutant swam at a rate that was slightly, but significantly, higher than wild type (107%) (Figure 10). However, two combinations of *strn-1 sad-1* doubles swam significantly slower than the corresponding *strn-1* singles (68 and 74%, respectively), suggesting that Sentryn and SAD kinase have at least one nonoverlapping function that affects locomotion (Figure 10). We note that, on solid media plates, where animals exhibit locomotion rates that average ∼1/6th of their rates in liquid, mutants lacking Sentryn and/or SAD kinase appear indistinguishable from wild type (data not shown). Overall, these relatively mild defects in locomotion suggest that the SV deficits at motor neuron synapses in these mutants are not large enough to profoundly affect the animal's behavior, and that there could be more than one SV capture mechanism.

Discussion

This study suggests that Sentryn is a novel active zone protein and a component of a sophisticated system that guides the transport and stable accumulation of SVs in the synaptic region. Evidence for a connection between Sentryn and the CSS system came from the finding that Sentryn and CSS system mutants affect DCV axonal transport and synaptic capture as part of the same system (Morrison *et al.* 2018). However, it was unclear whether Sentryn is merely an adaptor that connects the CSS system specifically to the guided transport and capture of DCVs, or whether it is a component of the CSS system in other contexts as well.

The results presented here suggest that, in most contexts, Sentryn is indeed a component of the CSS system because it can guide and regulate the motorized transport of a wide spectrum of cargos in neurons. These findings add to a growing body of evidence that the guided axonal transport of SVs and their stable accumulation in the synaptic region are linked through CSS system proteins.

We also provided evidence that Sentryn, like other CSS system proteins, is an active zone-enriched protein that contributes to the structure of the active zone. Sentryn, and the recently reported Clarinet protein (Xuan *et al.* 2017), appear to be the first active zone proteins to be discovered in over 11 years. The CSS system appears to be a specialized subset of active zone-enriched proteins that functions not only in the synaptic region, but throughout the neuron. Below, we expand on these concepts and explain their significance.

multi-bouton images were all acquired from different animals. Note that the highly focal localization of Sentryn-GFP is greatly disrupted in the *syd-2* null mutant. The scaling of these images has been altered by ∼50% to brighten the images for viewing the nonfocal localization. Sentryn appears to fill boutons, but is no longer enriched at the ventral apex where the active zone is located. As shown in the single bouton enlargements, Sentryn sometimes shows a patchy diffuse localization in *syd-2* mutant boutons. In *sad-1* mutant boutons, Sentryn localization appears partially disrupted, sometimes localizing to the ventral apex and sometimes appearing unlocalized or localizing to bouton regions other than the ventral apex. In general, Sentryn localization is variable in mutants lacking *sad-1*. To illustrate the scope of the variability, a panel of images of Sentryn localization in the *sad-1* null mutant is shown in Figure S6.

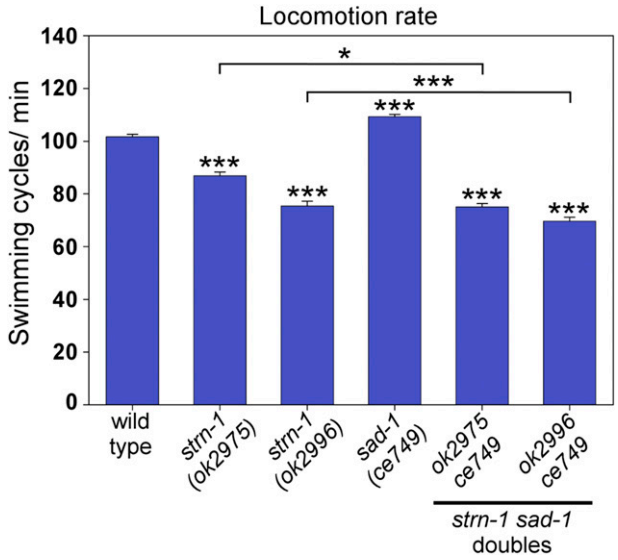

Figure 10 Sentryn mutations impair locomotion behavior. Swimming cycles per minute of the indicated genotypes. Data are means and SEMs from 72 wild type animals (~20,000 swimming cycles) and 36 animals for each mutant strain. *, ***: $P < 0.05$, $P < 0.0001$, respectively, when compared to wild type, or when comparing the indicated two strains.

Sentryn and CSS system mutants can affect the active transport of a wide spectrum of cargos

Mutants lacking Sentryn have the signature spectrum of active transport phenotypes shared by all CSS system proteins. Active transport phenotypes in Sentryn and CSS system mutants present as a skewing of cargo distribution toward microtubule minus ends, away from axons and toward cell somas and dendrites. These phenotypes are unlikely to result from defects in neuronal polarity (*i.e.*, causing the dendrite to acquire the identity of an axon) for two reasons. First, defects in active transport can account for the altered distribution. Second, if the dendrite acquired the identity of an axon in CSS system mutants, the microtubule polarity of the dendrite would switch from predominantly minus-end out, as is the case for *C. elegans* motor neurons, to plus-end out. Impairing dynein would then worsen the accumulation of cargos in dendrites rather than mitigate this phenotype as we found (this study; Edwards *et al.* 2015a,b; Morrison *et al.* 2018 for DCVs).

The affected cargos include not only SVs and DCVs but also some classes of large cell soma organelles, such as lysosomes and early endosomes. Sentryn mutants, like CSS system mutants, exhibit a dynein-dependent accumulation of these organelles in dendrites, but only in an *unc-16*(−) (JIP3 null) background. To our knowledge, CSS system mutants are the only mutants that affect organelle transport in this manner. This is significant because it suggests that Sentryn and CSS system proteins can guide the active transport of cargos at locations far from the main site of enrichment of CSS proteins at active zones.

According to our current model, the core purpose of Sentryn and the CSS system in axonal regions proximal to the first synapse is to ensure that KIF1A outcompetes dynein, and, thus, promotes the forward progress of SVs and DCVs toward the synaptic region. Dynein is a constant threat to SVs and DCVs traveling to the synaptic region, causing them to reverse their direction numerous times en route (Edwards *et al.* 2015b).

The CSS system appears to have the ability to regulate transport in both directions, perhaps depending on the location, the cargo type, and the relative concentrations of each CSS protein within the axon. During guided transport of DCVs (and presumably SVs that are transported by the same motors), SYD-2 (Liprin-α), Sentryn, and SAD kinase all act to reduce pausing in the axon initial segment and in the synaptic region (Goodwin and Juo 2013; Morrison *et al.* 2018). The CSS system normally inhibits dynein-mediated movements in this context, without significantly affecting plus end-directed movements (Edwards *et al.* 2015a). In contrast, Sentryn and SAD Kinase promote KIF1A plus-end movements without affecting dynein minus-end movements (Morrison *et al.* 2018).

Consistent with SV transport being regulated similar to DCV transport, SYD-2 (Liprin-α) promotes the plus-end movements of the KIF1A plus-end motor itself (Wagner *et al.* 2009). After transport, as SVs become captured in the synaptic region, where CSS proteins are present in their highest concentrations, transport of DCVs and SVs is inhibited in both directions as DCVs and SVs decrease their exit frequencies from mature clusters (Wu *et al.* 2013; Morrison *et al.* 2018). In the synaptic region, Sentryn and SAD kinase also act to ensure balanced movement of any DCVs that spontaneously escape capture. Evidence for this comes from the finding that mutants lacking Sentryn and/or SAD kinase show a strong bias for DCV movements in the anterograde direction, which would take DCVs past the synaptic region (Morrison *et al.* 2018).

The guided active transport of SVs and their subsequent stable accumulation in the synaptic region may be mechanistically linked through sentryn, SAD kinase, and Liprin-α

Our results suggest that Sentryn acts with SAD kinase and Liprin-α to ensure the stable accumulation of SVs in the synaptic region. The finding that Sentryn, SAD kinase, and Liprin-α are all involved in both SV guided transport and SV stable accumulation in the synaptic region is significant, because it suggests that both processes are linked through these proteins. Similar findings were also obtained for DCVs (Morrison *et al.* 2018). SYD-1 is also a CSS system protein and active zone component that functions in the same processes as Liprin-α and SAD kinase (Dai *et al.* 2006; Patel *et al.* 2006; Owald *et al.* 2010; Li *et al.* 2014; Edwards *et al.* 2015a). The common link seems to be the regulation of motor activity and/or the interactions of SVs with motors and/or microtubules.

The transport-to-capture transition

During transport, the effectiveness of dynein must be limited or overcome to allow the forward transport of SVs to dominate.

Upon reaching the synaptic region, a drastic transition occurs. SVs must be protected from counter-productive motor activity to be maintained in a captured state in clusters. However, SVs must now also be protected from plus end-directed movements, which would take them beyond the synaptic region.

We do not yet know how Sentryn and the CSS system alter their relationship with the motor system at the transport-to-capture transition. SYD-2 prevents the dissociation of SVs from clusters (Wu *et al.* 2013). To do so, SYD-2 would have to suppress movements in both directions, in contrast to the situation during transport where SYD-2 ensures the dominance of anterograde movements. In addition, in the absence of a CSS system SVs and DCVs accumulate in the distal asynaptic region, as far as ~0.5 mm from the synaptic region (Edwards *et al.* 2015b; this study; Morrison *et al.* 2018). Finally, Sentryn promotes entry into the synaptic region, and both Sentryn and SAD kinase strongly limit the number of both anterograde and retrograde movements of DCVs within the synaptic region (Morrison *et al.* 2018). Sentryn and SAD kinase also ensure balanced anterograde and retrograde movements for any DCVs that escape capture, favoring the recapture of DCVs in the synaptic region (Morrison *et al.* 2018). Thus, CSS system proteins suppress unbalanced plus- and minus-end movements after capture, but they primarily ensure the dominance of plus-end movements during transport.

One possible explanation for the transport-to-capture transition is that the much higher concentrations of CSS system proteins in the synaptic region (*i.e.*, their strong enrichment near active zones) alters their interactions with the motor system and ultimately leads to the inhibition of motorized transport. Interestingly, our EM data suggest that Sentryn and SAD kinase are not necessary to capture or retain SVs closer than 165 nm from the DP, but they are required to capture or retain more distal SVs. This suggests that capture may be a two-step process. The first step or mechanism, mediated by CSS proteins, appears to promote capture of SVs that are 165–700 nm from the active zone. The second step promotes the capture of SVs more proximal to the active zone (<165 nm). It is possible that one or both of these mechanisms utilize physical anchoring or tethering, such as to the DP or filaments emanating from it. However, mutant mice axons that lack active zones and DPs still contain wild type levels of Liprin-α (SYD-2) at synapses and still capture wild-type numbers of SVs that are unclustered (Acuna *et al.* 2016; Wang *et al.* 2016). Although this does not rule out that some form of tethering contributes to capture, it suggests that immobilization via physical anchoring to the DP is not necessary for the SV capture. Tethering of SVs at synapses may act primarily to cluster SVs or reduce the diffusion of SVs from synaptic sites, but further investigation is necessary to determine whether tethering is sufficient to protect SVs from the strong forces of motors.

Visualizing SV accumulation defects in different kinds of axons

SV accumulation defects can be difficult to detect in some neurons. The DA9 motor neuron in *C. elegans* is ideal for visualizing such defects because it has a compact synaptic region and a long, distal asynaptic region. The defects we observed in in *sad-1* and *strn-1* mutants sublateral motor neuron axons, which have a very different arrangement of SV clusters compared to DA9, are consistent with the defects we observed in the DA9 neuron. In both cases, in CSS system mutants, SV clusters are smaller in size, and SVs accumulate in asynaptic regions.

Sentryn appears to be a novel active zone protein and a missing link enabling the function of SYD-2 (Liprin-α) in the synaptic region

In the synaptic region, analysis of double and triple mutants showed that Sentryn and SAD kinase each have at least one nonoverlapping function that, when combined with their shared functions, enables most of the functions of SYD-2 (Liprin-α) for ensuring optimal levels of SVs in the synaptic region. We also observed Sentryn and SAD kinase additive effects for DCV accumulation in the synaptic region of cholinergic motor neurons. The additive effects of Sentryn and SAD kinase are significant because it has long been known that SYD-2 acts in the same pathway as SAD kinase for synapse assembly and capturing SVs to clusters (Patel *et al.* 2006). However, mutants lacking SYD-2 have significantly stronger synapse assembly/SV capture phenotypes than mutants lacking SAD kinase (Patel *et al.* 2006; Edwards *et al.* 2015b). This led to the prediction that one or more additional SYD-2 effectors exists (Patel *et al.* 2006). Our results suggest that Sentryn is the missing effector.

We observed no additive effects for Sentryn and SAD kinase for their functions in excluding lysosomes and SVs from dendrites. These findings further support the concept that the relationships of CSS proteins to the motor system differ in different contexts or regions of the neuron, as has also been shown for DCVs (Morrison *et al.* 2018).

This study suggests that Sentryn is an active zone protein. This is significant because active zone proteins are not frequently discovered. Sentryn and the recently discovered Clarinet protein (Xuan *et al.* 2017) appear to be the first new active zone proteins to be discovered in many years. Adding mechanistic insight into the actions of Sentryn, we showed that Sentryn is dependent on SYD-2 (Liprin-α) for its localization to active zones. Similar results have been found for SAD Kinase (Patel *et al.* 2006). Thus, at active zones, Sentryn and SAD kinase act downstream of SYD-2 and must at some point physically interact with SYD-2 (Liprin-α), or with a SYD-2-dependent protein or complex, to mediate the active zone functions of SYD-2. However, the interaction of Sentryn with other proteins may be transient or unstable because Sentryn has eluded discovery by conventional biochemical approaches for over 25 years, despite very intensive investigation of SVs, DCVs, and active zone proteins by many laboratories.

The CSS system: a specialized set of active zone-enriched proteins

Our results suggest that not all active zone-enriched proteins have essential roles in the CSS system. This supports a growing

body of evidence suggesting that there are at least two groups of active zone-enriched proteins.

One appears to play a major role in active zone structure, but does not have a direct role in SV capture. This group was revealed by studies that found that dual elimination of either RIM plus RIMB protein or ELKS plus RIM led to disassembly of the active zone/DP and eliminated tethering and priming (*i.e.*, docking) of SVs but did not affect SV capture at synapses (Acuna *et al.* 2016; Wang *et al.* 2016). This first group may also include other structural components of the active zone that together mediate several different functions related to neurotransmitter release, such as Ca^{2+} channel localization and function and SV docking (Sudhof 2012; Ackermann *et al.* 2015). The second group of active zone proteins, represented by CSS proteins, appears to play a minor structural role in determining the length of the DP, but mainly functions in capturing vesicles in the 165–700 nm zone relative to the DP. In *Drosophila* mutants lacking both SYD-1 and SYD-2 (Liprin-α), and in worm mutants lacking SYD-2, the active zone/DP (known as a T-bar in flies) is "readily identifiable" (Owald *et al.* 2010; Stigloher *et al.* 2011), although quantitative studies in *C. elegans* have shown that the DP can be significantly shorter in CSS system mutants, at least at cholinergic motor neuron synapses (Kittelmann *et al.* 2013; this study).

The CSS system is the specialized set of active-zone enriched proteins that has dual roles in both guiding the active transport of SVs and DCVs and in ensuring their capture/stable accumulation in the synaptic region. It is important to note that "active zone-enriched" does not mean that the proteins exclusively localize to, or exclusively function at, the active zone. CSS system proteins also affect transport at sites far removed from active zones in the synaptic region. Furthermore, because DCVs do not share as close a relationship with active zones as SVs, and yet are captured to the synaptic region with the same fidelity as SVs (Morrison *et al.* 2018), we hypothesize that Sentryn, SAD kinase, and Liprin-α are also present at the sites of DCV capture (*i.e.*, on the fringes of the SV cluster), but that they are greatly enriched at active zones (*i.e.*, at the center of the SV cluster).

Originally the CSS system was named for three founder proteins (CDK-5, SAD-1, and SYD-2) that inhibit dynein-mediated lysosome clearance in *unc-16* mutant axons (Edwards *et al.* 2015a). However, CDK-5 does not strictly fit this definition, because, even though it promotes the outward transport of SVs and DCVs (and organelles in the absence of *unc-16*) (Ou *et al.* 2010; Goodwin *et al.* 2012; Edwards *et al.* 2015a,b), there is no evidence that it is enriched at active zones or that it participates in SV capture. Indeed, in *cdk-5* null mutants SV clusters do not expand into the distal asynaptic region (synaptic region length 95 ± 15% of wild type; $N = 14$). Hence, in this article we have proposed redefining the CSS abbreviation as *Core Synapse Stability* system to reflect its ultimate role of ensuring the transport and retention of optimal numbers of captured SVs and DCVs at synapses.

Acknowledgments

We thank Edwin Levitan for providing a plasmid containing Emerald, and Joshua Arribere and Andrew Fire for providing the gRNA plasmid pJP118. Many critical strains in this work were provided by the *Caenorhabditis* Genetics Center, which is funded by the National Institutes of Health (NIH) Office of Research Infrastructure Programs (P40 OD010440) and by Shohei Mitani as part of the Japanese National Bioresource Project. This work was supported by a grant from the National Institute of General Medical Sciences of the NIH (R01GM080765 to K.G.M.) and by a grant from the Oklahoma Center for the Advancement of Science and Technology (HR14-003 to K.G.M.). This work made use of the BioCryo facility of Northwestern University's NU*ANCE* Center, which has received support from the Soft and Hybrid Nanotechnology Experimental (SHyNE) Resource (NSF ECCS-1542205); the MRSEC program (NSF DMR-1720139) at the Materials Research Center; the International Institute for Nanotechnology (IIN); and the State of Illinois, through the IIN. It also made use of the CryoCluster equipment, which has received support from the Major Research Instrumentation (MRI) program (NSF DMR-1229693).

Note added in proof: See Morrison *et al.* 2018 (pp 925–946) in this issue for a related work.

Literature Cited

Ackley, B. D., R. J. Harrington, M. L. Hudson, L. Williams, C. J. Kenyon *et al.*, 2005 The two isoforms of the Caenorhabditis elegans leukocyte-common antigen related receptor tyrosine phosphatase PTP-3 function independently in axon guidance and synapse formation. J. Neurosci. 25: 7517–7528.

Ackermann, F., C. L. Waites, and C. C. Garner, 2015 Presynaptic active zones in invertebrates and vertebrates. EMBO Rep 16: 923–938.

Acuna, C., X. Liu, and T. C. Sudhof, 2016 How to make an active zone: unexpected universal functional redundancy between RIMs and RIM-BPs. Neuron 91: 792–807. https://doi.org/10.1016/j.neuron.2016.07.042

Alfonso, A., K. Grundahl, J. S. Duerr, H.-P. Han, and J. B. Rand, 1993 The *Caenorhabditis elegans unc-17* gene: a putative vesicular acetylcholine transporter. Science 261: 617–619.

Arribere, J. A., R. T. Bell, B. X. Fu, K. L. Artiles, P. S. Hartman *et al.*, 2014 Efficient marker-free recovery of custom genetic modifications with CRISPR/Cas9 in Caenorhabditis elegans. Genetics 198: 837–846. https://doi.org/10.1534/genetics.114.169730

Baas, P. W., and S. Lin, 2011 Hooks and comets: the story of microtubule polarity orientation in the neuron. Dev. Neurobiol. 71: 403–418. https://doi.org/10.1002/dneu.20818

Brenner, S., 1974 The genetics of *C. elegans*. Genetics 77: 71–94.

Burton, P. R., and J. L. Paige, 1981 Polarity of axoplasmic microtubules in the olfactory nerve of the frog. Proc. Natl. Acad. Sci. USA 78: 3269–3273.

Chalfie, M., and J. White, 1988 The nervous system, pp. 337–391 in *The Nematode Caenorhabditis elegans*, edited by W. B. Wood. Cold Spring Harbor Laboratory Press, Cold Spring Harbor, NY.

Charlie, N. K., M. A. Schade, A. M. Thomure, and K. G. Miller, 2006 Presynaptic UNC-31 (CAPS) is required to activate the G alpha(s) pathway of the Caenorhabditis elegans synaptic signaling network. Genetics 172: 943–961.

Crump, J. G., M. Zhen, Y. Jin, and C. I. Bargmann, 2001 The SAD-1 kinase regulates presynaptic vesicle clustering and axon termination. Neuron 29: 115–129.

Dai, Y., H. Taru, S. L. Deken, B. Grill, B. Ackley *et al.*, 2006 SYD-2 Liprin-alpha organizes presynaptic active zone formation through ELKS. Nat. Neurosci. 9: 1479–1487.

Dickinson, D. J., J. D. Ward, D. J. Reiner, and B. Goldstein, 2013 Engineering the Caenorhabditis elegans genome using Cas9-triggered homologous recombination. Nat. Methods 10: 1028–1034. https://doi.org/10.1038/nmeth.2641

Edwards, S. L., N. K. Charlie, M. C. Milfort, B. S. Brown, C. N. Gravlin *et al.*, 2008 A novel molecular solution for ultraviolet light detection in Caenorhabditis elegans. PLoS Biol. 6: e198. https://doi.org/10.1371/journal.pbio.0060198

Edwards, S. L., S. C. Yu, C. M. Hoover, B. C. Phillips, J. E. Richmond *et al.*, 2013 An organelle gatekeeper function for Caenorhabditis elegans UNC-16 (JIP3) at the axon initial segment. Genetics 194: 143–161. https://doi.org/10.1534/genetics.112.147348

Edwards, S. L., L. M. Morrison, R. M. Yorks, C. M. Hoover, S. Boominathan *et al.*, 2015a UNC-16 (JIP3) acts through synapse-assembly proteins to inhibit the active transport of cell soma organelles to Caenorhabditis elegans motor neuron axons. Genetics 201: 117–141. https://doi.org/10.1534/genetics.115.177345

Edwards, S. L., R. M. Yorks, L. M. Morrison, C. M. Hoover, and K. G. Miller, 2015b Synapse-assembly proteins maintain synaptic vesicle cluster stability and regulate synaptic vesicle transport in Caenorhabditis elegans. Genetics 201: 91–116. https://doi.org/10.1534/genetics.115.177337

Fernandez-Busnadiego, R., B. Zuber, U. E. Maurer, M. Cyrklaff, W. Baumeister *et al.*, 2010 Quantitative analysis of the native presynaptic cytomatrix by cryoelectron tomography. J. Cell Biol. 188: 145–156. https://doi.org/10.1083/jcb.200908082

Fouquet, W., D. Owald, C. Wichmann, S. Mertel, H. Depner *et al.*, 2009 Maturation of active zone assembly by Drosophila Bruchpilot. J. Cell Biol. 186: 129–145. https://doi.org/10.1083/jcb.200812150

Goodwin, P. R., and P. Juo, 2013 The scaffolding protein SYD-2/Liprin-alpha regulates the mobility and polarized distribution of dense-core vesicles in C. elegans motor neurons. PLoS One 8: e54763. https://doi.org/10.1371/journal.pone.0054763

Goodwin, P. R., J. M. Sasaki, and P. Juo, 2012 Cyclin-dependent kinase 5 regulates the polarized trafficking of neuropeptide-containing dense-core vesicles in Caenorhabditis elegans motor neurons. J. Neurosci. 32: 8158–8172. https://doi.org/10.1523/JNEUROSCI.0251-12.2012

Hall, D. H., and E. M. Hedgecock, 1991 Kinesin-related gene unc-104 is required for axonal transport of synaptic vesicles in C. elegans. Cell 65: 837–847.

Hallam, S. J., A. Goncharov, J. McEwen, R. Baran, and Y. Jin, 2002 SYD-1, a presynaptic protein with PDZ, C2 and rhoGAP-like domains, specifies axon identity in C. elegans. Nat. Neurosci. 5: 1137–1146.

Hammarlund, M., S. Watanabe, K. Schuske, and E. M. Jorgensen, 2008 CAPS and syntaxin dock dense core vesicles to the plasma membrane in neurons. J. Cell Biol. 180: 483–491. https://doi.org/10.1083/jcb.200708018

Heidemann, S. R., J. M. Landers, and M. A. Hamborg, 1981 Polarity orientation of axonal microtubules. J. Cell Biol. 91: 661–665.

Hoover, C. M., S. L. Edwards, S. C. Yu, M. Kittelmann, J. E. Richmond *et al.*, 2014 A novel CaM kinase II pathway controls the location of neuropeptide release from Caenorhabditis elegans motor neurons. Genetics 196: 745–765. https://doi.org/10.1534/genetics.113.158568

Inoue, E., S. Mochida, H. Takagi, S. Higa, M. Deguchi-Tawarada *et al.*, 2006 SAD: a presynaptic kinase associated with synaptic vesicles and the active zone cytomatrix that regulates neurotransmitter release. Neuron 50: 261–275.

Kandel, E. R., 2013 *Principles of Neural Science*. McGraw-Hill, New York.

Kittelmann, M., J. Hegermann, A. Goncharov, H. Taru, M. H. Ellisman *et al.*, 2013 Liprin-alpha/SYD-2 determines the size of dense projections in presynaptic active zones in C. elegans. J. Cell Biol. 203: 849–863. https://doi.org/10.1083/jcb.201302022

Klassen, M. P., and K. Shen, 2007 Wnt signaling positions neuromuscular connectivity by inhibiting synapse formation in *C. elegans*. Cell 130: 704–716.

Landis, D. M., A. K. Hall, L. A. Weinstein, and T. S. Reese, 1988 The organization of cytoplasm at the presynaptic active zone of a central nervous system synapse. Neuron 1: 201–209.

Levitan, E. S., 2008 Signaling for vesicle mobilization and synaptic plasticity. Mol. Neurobiol. 37: 39–43. https://doi.org/10.1007/s12035-008-8014-3

Li, L., X. Tian, M. Zhu, D. Bulgari, M. A. Bohme *et al.*, 2014 Drosophila Syd-1, liprin-alpha, and protein phosphatase 2A B' subunit Wrd function in a linear pathway to prevent ectopic accumulation of synaptic materials in distal axons. J. Neurosci. 34: 8474–8487. https://doi.org/10.1523/JNEUROSCI.0409-14.2014

Mello, C. C., J. M. Kramer, D. Stinchcomb, and V. Ambros, 1991 Efficient gene transfer in *C. elegans*: extrachromosomal maintenance and integration of transforming sequences. EMBO J. 10: 3959–3970.

Miller, K. E., J. DeProto, N. Kaufmann, B. N. Patel, A. Duckworth *et al.*, 2005 Direct observation demonstrates that Liprin-alpha is required for trafficking of synaptic vesicles. Curr. Biol. 15: 684–689.

Miller, K. G., 2017 Keeping neuronal cargoes on the right track: new insights into regulators of axonal transport. Neuroscientist 23: 232–250.

Miller, K. G., A. Alfonso, M. Nguyen, J. A. Crowell, C. D. Johnson *et al.*, 1996 A genetic selection for Caenorhabditis elegans synaptic transmission mutants. Proc. Natl. Acad. Sci. USA 93: 12593–12598.

Miller, K. G., M. D. Emerson, and J. B. Rand, 1999 Goalpha and diacylglycerol kinase negatively regulate the Gqalpha pathway in C. elegans. Neuron 24: 323–333.

Morrison, L. M., S. L. Edwards, L. Manning, N. Stec, J. E. Richmond *et al.*, 2018 Sentryn and SAD Kinase Link the Guided Transport and Capture of Dense Core Vesicles in *Caenorhabditis elegans*. Genetics 210: 925–946.

Nicholls, J. G., 2012 *From Neuron to Brain*. Sinauer Associates, Sunderland, MA.

Ou, C. Y., V. Y. Poon, C. I. Maeder, S. Watanabe, E. K. Lehrman *et al.*, 2010 Two cyclin-dependent kinase pathways are essential for polarized trafficking of presynaptic components. Cell 141: 846–858. https://doi.org/10.1016/j.cell.2010.04.011

Owald, D., W. Fouquet, M. Schmidt, C. Wichmann, S. Mertel *et al.*, 2010 A Syd-1 homologue regulates pre- and postsynaptic maturation in Drosophila. J. Cell Biol. 188: 565–579. https://doi.org/10.1083/jcb.200908055

Paix, A., Y. Wang, H. E. Smith, C. Y. Lee, D. Calidas *et al.*, 2014 Scalable and versatile genome editing using linear DNAs with microhomology to Cas9 sites in Caenorhabditis elegans. Genetics 198: 1347–1356. https://doi.org/10.1534/genetics.114.170423

Patel, M. R., E. K. Lehrman, V. Y. Poon, J. G. Crump, M. Zhen *et al.*, 2006 Hierarchical assembly of presynaptic components in defined C. elegans synapses. Nat. Neurosci. 9: 1488–1498.

Reynolds, N. K., M. A. Schade, and K. G. Miller, 2005 Convergent, RIC-8-dependent Galpha signaling pathways in the Caenorhabditis elegans synaptic signaling network. Genetics 169: 651–670.

Schade, M. A., N. K. Reynolds, C. M. Dollins, and K. G. Miller, 2005 Mutations that rescue the paralysis of Caenorhabditis elegans ric-8 (synembryn) mutants activate the G alpha(s) pathway and define a third major branch of the synaptic signaling network. Genetics 169: 631–649.

Siksou, L., P. Rostaing, J. P. Lechaire, T. Boudier, T. Ohtsuka *et al.*, 2007 Three-dimensional architecture of presynaptic terminal cytomatrix. J. Neurosci. 27: 6868–6877.

Sossin, W. S., and R. H. Scheller, 1991 Biosynthesis and sorting of neuropeptides. Curr. Opin. Neurobiol. 1: 79–83.

Stiernagle, T., 2006 Maintenance of C. elegans (February 11, 2006), *WormBook*, ed. The *C. elegans* Research Community, WormBook, doi/10.1895/wormbook.1.101.1, http://www.wormbook.org.

Stigloher, C., H. Zhan, M. Zhen, J. Richmond, and J. L. Bessereau, 2011 The presynaptic dense projection of the Caenorhabditis elegans cholinergic neuromuscular junction localizes synaptic vesicles at the active zone through SYD-2/liprin and UNC-10/RIM-dependent interactions. J. Neurosci. 31: 4388–4396. https://doi.org/10.1523/JNEUROSCI.6164-10.2011

Sudhof, T. C., 2012 The presynaptic active zone. Neuron 75: 11–25.

Sulston, J., and J. Hodgkin, 1988 Methods, pp. 596–597 in *The Nematode Caenorhabditis elegans*, edited by W. B. Wood. Cold Spring Harbor Laboratory, Cold Spring Harbor, NY.

Wagner, O. I., A. Esposito, B. Kohler, C. W. Chen, C. P. Shen *et al.*, 2009 Synaptic scaffolding protein SYD-2 clusters and activates kinesin-3 UNC-104 in C. elegans. Proc. Natl. Acad. Sci. USA 106: 19605–19610.

Wang, S. S. H., R. G. Held, M. Y. Wong, C. Liu, A. Karakhanyan *et al.*, 2016 Fusion competent synaptic vesicles persist upon active zone disruption and loss of vesicle docking. Neuron 91: 777–791. https://doi.org/10.1016/j.neuron.2016.07.005

Weimer, R. M., 2006 Preservation of C. elegans tissue via high-pressure freezing and freeze-substitution for ultrastructural analysis and immunocytochemistry. Methods Mol. Biol. 351: 203–221.

Weimer, R. M., E. O. Gracheva, O. Meyrignac, K. G. Miller, J. E. Richmond *et al.*, 2006 UNC-13 and UNC-10/rim localize synaptic vesicles to specific membrane domains. J. Neurosci. 26: 8040–8047.

White, J. G., E. Southgate, J. N. Thomson, and S. Brenner, 1986 The structure of the nervous system of the nematode *Caenorhabditis elegans*. Philos. Trans. R. Soc. Lond. B Biol. Sci. 314: 1–340.

Wu, Y. E., L. Huo, C. I. Maeder, W. Feng, and K. Shen, 2013 The balance between capture and dissociation of presynaptic proteins controls the spatial distribution of synapses. Neuron 78: 994–1011. https://doi.org/10.1016/j.neuron.2013.04.035

Xuan, Z., L. Manning, J. Nelson, J. E. Richmond, D. A. Colon-Ramos *et al.*, 2017 Clarinet (CLA-1), a novel active zone protein required for synaptic vesicle clustering and release. eLife 6: pii: e29276. https://doi.org/10.7554/eLife.29276

Yan, J., D. L. Chao, S. Toba, K. Koyasako, T. Yasunaga *et al.*, 2013 Kinesin-1 regulates dendrite microtubule polarity in Caenorhabditis elegans. eLife 2: e00133. https://doi.org/10.7554/eLife.00133

Yeh, E., T. Kawano, R. M. Weimer, J. L. Bessereau, and M. Zhen, 2005 Identification of genes involved in synaptogenesis using a fluorescent active zone marker in *Caenorhabditis elegans*. J. Neurosci. 25: 3833–3841.

Zhen, M., and Y. Jin, 1999 The liprin protein SYD-2 regulates the differentiation of presynaptic termini in C. elegans. Nature 401: 371–375.

Zheng, Q., S. Ahlawat, A. Schaefer, T. Mahoney, S. P. Koushika *et al.*, 2014 The vesicle protein SAM-4 regulates the processivity of synaptic vesicle transport. PLoS Genet. 10: e1004644. https://doi.org/10.1371/journal.pgen.1004644

Communicating editor: M. Johnston